LRP 173/80 October 1980

# ELECTROMAGNETIC RADIATION FROM AN INHOMOGENEOUS PLASMA : THEORY AND EXPERIMENT

R.W. Means, L. Muschietti, M.Q. Tran, and J. Vaclavik

# Electromagnetic Radiation from an Inhomogeneous Plasma: Theory and Experiment

R.W. Means, L. Muschietti, M.Q. Tran, and J. Vaclavik

Centre de Recherches en Physique des Plasmas
Association Euratom - Confédération Suisse
Ecole Polytechnique Fédérale de Lausanne
CH-1007 Lausanne / Switzerland

ABSTRACT

The problem of linear conversion of a Langmuir wave (L) to a transverse electromagnetic wave (T) in the presence of a density gradient has been solved numerically with appropriate boundary conditions. A reciprocity principle was found, allowing the deduction of solutions of this problem from those obtained from the conversion TL. We have applied this model to study the spectrum emitted from an inhomogeneous plasma, including the effect of the antenna radiation pattern. Experiments have been performed in a large unmagnetized d.c. discharge plasma ($n_e \sim 5\ 10^{10} cm^{-3}$, $T_e = 1.3$ eV, gradient scale length L = 100 - 1000 cm). The shape of the spectrum observed with a horn antenna agrees with the theoretical one, but the deduced level of L fluctuations is much higher than the thermal level. This enhancement is due to the presence of primary energetic ($E \approx 60$ eV) electrons.

## I. INTRODUCTION

The linear conversion of an electromagnetic wave into an electrostatic wave and the inverse conversion is of great importance for plasma physics and astrophysics. In a field-free plasma, a density inhomogeneity can couple the electromagnetic (T) wave into a Langmuir (L) wave. The problem of the conversion of a T wave into a L wave (in short the TL conversion) has been discussed by many authors.[1-8] The inverse problem, namely the conversion of a Langmuir wave into an electromagnetic wave, has been much less considered. Ginzburg,[1] after his discussion about the TL conversion, mentioned the possible importance of this phenomenon in the solar corona but made no further comments. Tidman[9] has computed the efficiency of the LT coupling in the WKB approximation. However, due to the WKB approximation, the behavior of the waves near the turning point was not treated.

Experimentally, Stenzel et al.[10] have studied the linear TL conversion in the presence of a density gradient. The linear LT conversion has not been investigated. As mentioned previously, it has been speculated that this phenomenon could be responsible for ele
radiation from the solar corona.[1] In laboratory experi
served radiation near the plasma frequency has b
pret. Some authors[12-16] have attempted t
thermal emission seen at the plasma frequ
to conversion from the L wave into the T wav

The present study deals with both the theoretical and the experimental aspect of the conversion of an L wave into a T wave in an inhomogeneous field-free plasma. The theory of this conversion is presented in Sec. II. In Sec. III we compute the electromagnetic power emitted from an inhomogeneous plasma, assuming an equilibrium distribution of plasmons. In Sec. IV, we discuss the experimental results obtained in our large field-free plasma device. A summary is then presented in Sec. V.

## II. THEORY OF LINEAR CONVERSION

When an electromagnetic wave is obliquely incident on an inhomogeneous plasma, it can be absorbed resonantly by linear mode conversion[1] into a plasma wave if its polarization lies in the plane of incidence. As the electrons oscillate with the electric field, one component of their motion lies along the gradient and causes an electrostatic charge separation so that the wave cannot remain purely electromagnetic. If the charge separation occurs at the natural frequency $\omega_p$, a Langmuir wave may appear. This classical problem has been considered in a new frame which allows to treat both transverse-Langmuir (TL) and Langmuir-transverse (LT) conversions.

A. Formulation of the problem

Let us consider the situation sketched in Fig. 1. In the half-space at left ($X < 0$), the density of the plasma is constant. Here the WKB method may be applied a fortiori so that the two modes, Langmuir wave and transverse wave, are well separated. They are simply described by their dispersion relations :

$$k_L^2 = \frac{\omega^2 - \omega_p^2}{3\beta c^2} - k_y^2 \qquad (1),$$

$$k_T^2 = \frac{\omega^2 - \omega_p^2}{c^2} - k_y^2 \qquad (2),$$

where $k_L$ ($k_T$) is the X-component of the wave vector $\vec{k}$ of the Langmuir wave (transverse wave); c is the velocity of light and $\beta$ is the ratio of electron thermal to rest mass energy, $\beta = v_e^2/c^2$.

In the half-space at right ($X > 0$), however, we have to solve the coupled differential equations for the electric field that come from the linearized electron Euler equations combined with Maxwell's equations[2] :

$$3\beta \frac{d^2 E_x}{dx^2} - (1-3\beta) i k_y \frac{d}{dx} E_y + \left( \frac{\omega^2 - \omega_p^2}{c^2} - k_y^2 \right) E_x = 3\beta\, \mathrm{re} \left( \frac{d}{dx} E_x + i k_y E_y \right) \qquad (3),$$

$$\frac{d^2}{dx^2} E_y - (1-3\beta) i k_y \frac{d}{dx} E_x + \left( \frac{\omega^2 - \omega_p^2}{c^2} - 3\beta k_y^2 \right) E_y = 0 \qquad (4).$$

Here $\mathscr{L}$ characterizes the inhomogenity of the background density and is related to the varying electron plasma frequency $\omega_{pe}$ by $\mathscr{L} = \frac{1}{\omega_{pe}^2} \frac{d}{dX} (\omega_{pe}^2)$. Even if the gradient is small, the wavelength is always of the same order as the density gradient scale length near the turning points, i.e., $\mathscr{L} \gtrsim k$ so that the WKB method fails. There are, in fact, three singular points: namely, the turning point for the Langmuir wave $\omega_{pe}^2(X_L) = \omega^2 - 3\beta\, k_y^2 c^2$; the turning point for the transverse wave $\omega_{pe}^2(X_T) = \omega^2 - k_y^2 c^2$; and the critical point where the two waves interact $\omega_{pe}^2(X_o) = \omega^2$ (cf. Fig. 1). The simplest approach is to solve numerically the Eqs. (3) - (4) with appropriate boundary conditions.

The situation described here can apply to two problems. In the first case, we send a transverse wave of p-polarization from $X = -\infty$; it is reflected at $X_T$ while a part of its energy reaches $X_0$ and comes back via a Langmuir wave (TL problem). In the second problem the roles played by the transverse and the Langmuir wave are exchanged (LT problem). In either case, the problem has three waves: one ingoing wave of either transverse or Langmuir type and two outgoing waves, one of each type. The transition from one problem to the other is carried out by a simple change in the boundary conditions associated with the pair of differential equations (3) - (4). The functions $E_X(X)$, $E_Y(X)$ are continuous at $X = 0$, since there is only one medium. By means of Maxwell's and Euler's equations it may easily be shown that their derivatives must also be continuous. The boundary conditions for the

TL and LT problems will be discussed separately.

Let us first consider the TL problem. In the half-space at left, $E_Y$ is given by the decomposition :

$$E_y = \exp(ik_T x) + R_T \exp(-ik_T x) + T_L \exp(-ik_L x) \quad , \quad x < o \tag{5}$$

By application of div $\underline{E} = 0$ for the transverse part and curl $\underline{E} = 0$ for the longitudinal part we get

$$E_x = \frac{k_y}{k_T}\left[ R_T \exp(-ik_T x) - \exp(ik_T x)\right] - \frac{k_L}{k_y} T_L \exp(-ik_L x) \quad , \quad x < o \tag{6}.$$

Simple algebra gives the coefficients of reflection $R_T$ and transmission $T_L$ as functions of the fields evaluated at $X = 0_-$ .

$$R_T = \frac{k_L k_T}{k_y^2 + k_L k_T}\left[ E_y(0_-) + \frac{k_y}{k_L} E_x(0_-) + \frac{k_y^2}{k_L k_T} - 1 \right] \tag{7},$$

$$T_L = \frac{k_y k_T}{k_y^2 + k_L k_T}\left[ \frac{k_y}{k_T} E_y(0_-) - E_x(0_-) - 2\frac{k_y}{k_T} \right] \tag{8}.$$

Anticipating Sec. II B where the differential problem will be transformed into its weak variational form, we will seek boundary conditions for the derivatives. We therefore differentiate Eq. (5) and evaluate the resulting expression by means of Eqs. (7) and (8). The transcription of the expression for $X = 0_+$ is then trivial,

$$\frac{d}{dx} E_y(0_+) = \frac{i}{k_y^2 + k_L k_T} \left[ E_x(0_+) k_y k_T (k_L - k_T) \right.$$
$$\left. - E_y(0_+) k_L (k_T^2 + k_y^2) + 2 k_L (k_y^2 + k_T^2) \right] \quad (9).$$

Repeating the same procedure for Eq. (6) we obtain

$$\frac{d}{dx} E_x(0_+) = \frac{i}{k_y^2 + k_L k_T} \left[ E_y(0_+) k_y k_L (k_L - k_T) \right.$$
$$\left. - E_x(0_+) k_T (k_L^2 + k_y^2) - 2 k_y (k_L^2 + k_y^2) \right] \quad (10).$$

Let us now consider the LT problem. The three waves are given by

$$E_y = \exp(i k_L x) + R_L \exp(-i k_L x) + T_T \exp(-i k_T x), \quad x < 0 \quad (11).$$

The same procedure is applied to this new starting point to give:

$$E_x = \frac{k_L}{k_y}\left[\exp(ik_L x) - R_L \exp(-ik_L x)\right] + \frac{k_y}{k_T} T_T \exp(-ik_T x) \quad , \; x < 0 \tag{12},$$

$$R_L = \frac{k_y k_T}{k_y^2 + k_L k_T}\left[\frac{k_y}{k_T} E_y(0_-) - E_x(0_-) + \frac{k_L}{k_y} - \frac{k_y}{k_T}\right] \tag{13},$$

$$T_T = \frac{k_y k_T}{k_y^2 + k_L k_T}\left[\frac{k_L}{k_y} E_y(0_-) + E_x(0_-) - 2\frac{k_L}{k_y}\right] \tag{14},$$

$$\frac{d}{dx} E_y(0_+) = \frac{i}{k_y^2 + k_L k_T}\left[E_x(0_+) k_y k_T (k_L - k_T) - E_y(0_+)(k_y^2 + k_T^2) k_L + 2k_L (k_y^2 + k_T^2)\right] \tag{15},$$

$$\frac{d}{dx} E_x(0_+) = \frac{i}{k_y^2 + k_L k_T}\left[E_y(0_+) k_y k_L (k_L - k_T) - E_x(0_+)\frac{k_T (k_y^2 + k_T^2)}{3\beta} - 2\frac{k_y}{3\beta}(k_y^2 + k_T^2)\right] + \frac{2i(k_T^2 + k_y^2)}{3\beta k_y} \tag{16}.$$

It is worth noting that the boundary conditions for the two problems are the same except for the last term in Eq. (16). Thus, in spite of their symmetry, the two problems are distinct.

The process of resonant absorption has been studied by many authors[1-8] either for a cold plasma or for a warm one. In the latter case, the situation is similar to our TL problem except for the finite density in the half-space at left. The approach used here, in our opinion, has the following advantage. We do not have to artificially damp the Langmuir wave generated in order to prevent it from propagating towards the boundary. Also, a simple rescaling allows us to formally eliminate the role of the finite density at the left from the equations, so that the classical situation may be recovered as a particular case.

Let us introduce the dimensionless variables $x = k_o X = \frac{\omega}{c} X$, $g(x) = \frac{1}{\omega^2} \omega_p^2(x)$, in Eqs. (3) and (4). Defining $k_y c/\omega = \sin\theta_o$, where $\theta_o$ is the angle that the transverse wave would make with respect to the gradient in the vacuum, we obtain just the standard equations,[2]

$$3\beta \frac{d^2}{dx^2} E_x - (1-3\beta) i \sin\theta_o \frac{d}{dx} E_y + (1 - g - \sin^2\theta_o) E_x = 3\beta \overline{\varkappa} \left( \frac{d}{dx} E_x + i \sin\theta_o E_y \right) ,$$

$$\frac{d^2}{dx^2} E_y - (1-3\beta) i \sin\theta_o \frac{d}{dx} E_x + (1 - g - 3\beta \sin^2\theta_o) E_y = 0 ,$$

where $\overline{\varkappa} = \frac{1}{n} \frac{dn}{dx}$, with n the background density.

Their solutions are associated historically with the parameter $q = (k_o L_c)^{2/3} \sin^2\theta_o$, where $k_o$ is the vacuum wave number and $L_c$ is the characteristic length of the profile in the vicinity of the critical density. For a linear profile this parameter allows us to summarize the results with respect to the absorption A(q) in only one graph (Fig. 2).

The vacuum case may be recovered from the TL problem by a re-scaling of the q-parameter so that our results can be compared with the classical studies. The natural parameters for the TL problem are :

i) the angle of the transverse wave with respect to the gradient in the homogeneous part of the space

$$\sin^2\theta = \frac{k_y^2}{k_y^2 + k_r^2} = \frac{k_y^2 c^2}{\omega^2(1-g_o)} = \frac{\sin^2\theta_o}{(1-g_o)} \quad ,$$

where $g_o = \omega_{p(o)}^2/\omega^2$ .

ii) the characteristic length of the profile measured with respect to the density of the homogeneous part

$$L = n(x=0)\Big/\frac{d}{dx}n(x=x_o) = L_c\ g_o$$

The parameter q may then be rewritten as

$$q = \left(\frac{\omega}{c} L \frac{1}{q_0}\right)^{2/3} \sin^2\theta (1 - q_0) = \left(\frac{\omega_{p_0} L}{c}\right)^{2/3} \sin^2\theta \left(\frac{\omega^2}{\omega_{p_0}^2} - 1\right) \qquad (17),$$

where $\omega_{po}$ stands for the electron plasma frequency at x = 0.

Since A(q) is a peaked function (Fig. 2), we see that, for a given linear profile and for a given angle, there exists an optimal frequency with regard to absorption and thus with regard to conversion into plasma waves.

Let us consider the energy flux of the waves. The equation for the transfer of energy associated with a wave packet is

$$\frac{\partial}{\partial t} \mathcal{E}_K + \operatorname{div}\left(\vec{V}_g \; \mathcal{E}_K\right) = 0 \qquad (18).$$

Here $\varepsilon_k$ is the energy density of the wave packet and $\vec{v}_g = \frac{d\omega}{d\vec{k}}$, the group velocity. The Poynting flux $\vec{S} = \vec{v}_g \; \varepsilon_k$ may be calculated simply once the mode (transverse or Langmuir) is specified. Its X-component is

$$S_x^T = \frac{|\bar{E}_y|^2}{8\pi} \frac{k^2 c^2}{k_x \omega} \tag{19}$$

for the transverse mode, and

$$S_x^L = \frac{|\bar{E}_y|^2}{8\pi} 3\beta \frac{k^2 c^2}{\omega k_y} \frac{k_x}{k_y} \tag{20}$$

for the Langmuir mode.

By evaluating the different fluxes that pass through the plane X = 0, we may define absorption coefficients

$$A_T^L = \frac{S_x^{iT} - S_x^{rT}}{S_x^{iT}} = 1 - |R_T|^2 \tag{21},$$

$$A_L^T = \frac{S_x^{iL} - S_x^{rL}}{S_x^{iL}} = 1 - |R_L|^2 \tag{22},$$

and emission coefficients

$$\mathcal{E}_T^L = \frac{S_x^{oL}}{S_x^{iT}} = |\bar{T}_L|^2 \frac{k_L k_T}{k_y^2} \tag{23},$$

$$\mathcal{E}_L^T = \frac{S_x^{oT}}{S_x^{iL}} = |T_T|^2 \frac{k_y^2}{k_L k_T} \tag{24}.$$

Here the superscripts i, r, o, refer to incident, reflected and outgoing respectively.

B. Numerical procedure

The value of the total electric field in each point is the superposition of the three waves involved. Those are specified by the boundary conditions Eqs. (9) and (10) (or (15) and (16)) at $X = 0$ together with conditions of evanescence at $X = \ell >> X_o$. Thus, the stationary problem described by the differential equations (3) and (4) has the character of a boundary value problem. A convenient way to treat this type of problem is to use the Ritz-Galerkin method together with a finite element scheme.[17] The boundary conditions are then introduced when integrating by parts the terms with second derivatives. Let us normalize the density by the critical density $n(x) = n(x_o)\, g(x)$, and the space by the wave vector of a transverse wave in the homogeneous part $(X < 0)$ $X = (k_Y^2 + k_T^2)^{-\frac{1}{2}}\, x$. Equations (3) and (4) then read

$$3\beta \ddot{E}_x - (1-3\beta)\, i \sin\theta\, \dot{E}_y + \left[ \frac{1-g}{1-g(0)} - \sin^2\theta \right] E_x$$

$$= 3\beta\varkappa \left( \dot{E}_x + i \sin\theta\, E_y \right) \qquad (25),$$

$$\ddot{E}_y - (1-3\beta)\, i \sin\theta\, \dot{E}_x + \left[ \frac{1-g}{1-g(0)} - 3\beta \sin^2\theta \right] E_y = 0 \qquad (26),$$

where the dot denotes the derivative with respect to x and $\mathcal{K}$ is redefined as $\mathcal{K} = \dot{n}/n$. For the boundary conditions at left one obtains from (9) and (10) - (15) and (16)

$$\dot{E}_x(0) = \frac{i}{k_L k_T + \sin^2\theta} \left[ E_y (k_L - k_T) k_L \sin\theta - E_x k_T/3\beta - 2\sin\theta/3\beta \right] + \Gamma \qquad (27),$$

$$\dot{E}_y(0) = \frac{i}{k_L k_T + \sin^2\theta} \left[ E_x (k_L - k_T) k_T \sin\theta - E_y k_L + 2 k_L \right] \qquad (28).$$

Here $\Gamma$ is the extra term which distinguishes the LT and the TL problem :

$$\Gamma = (3\beta \sin\theta/2)^{-1} \text{ for LT , and } \Gamma = 0 \text{ for TL .}$$

At right one has simply

$$E_x(\ell) = 0 \qquad (29),$$

$$E_y(\ell) = 0 \qquad (30).$$

The differential problem, Eqs. (25) - (30), was put into its weak variational form after splitting the complex equation into real equations and solved by means of a computer for the case of a finite functional space generated by the usual roof functions.

## C. Interpretation of the results

The four emission and absorption coefficients, Eqs. (21), (22), (23), and (24), were computed for different cases by varying the density profile, the incident angle, the temperature and the frequency. In view of the considerations made earlier, the coefficient $A_T^L$ was known independently for a linear profile[2] so that the operation of the code could be tested. Surprisingly, the emission coefficient $\varepsilon_T^L$ turned out to be different from $A_T^L$, although the medium was not dissipative. This fact is due to the work done on the oscillating electrons by the external force that maintains the density gradient. This extra work may be calculated analytically within the WKB-approximation, as we shall see later, via the damping-like effect which influences the propagation of a Langmuir wave in an inhomogeneous plasma. Although these features were useful to consistently interpret the numerical results of the TL problem, the most powerful result was found to be a reciprocity principle. This exact and general principle allowed us to confine ourselves to the study of one of the two problems only.

1. Principles of reciprocity and of local conversion

We propose now to demonstrate the following reciprocity principle :

$$A_L^T = A_T^L = A \qquad (31)$$

$$\varepsilon_L^T \quad \varepsilon_T^L = A^2 \qquad (32)$$

proof: by definition of the four emission and absorption coefficients, Eqs. (21) - (24), the statements (31) and (32) are equivalent to the following relations between the coefficients of the wave :

$$|R_L| = |R_T| \quad ,$$

$$|T_T|^2 \, |T_L|^2 = \left(1 - |R_T|^2\right)^2 \quad .$$

Let us now consider the following cycle, starting with a Langmuir wave of amplitude unity and phase zero (Fig. 3). After passing through the convertor, we obtain a Langmuir wave $|R_L|\exp(ir_L)$ and a transverse wave $|T_T|\exp(it_T)$. Both waves are reflected by a mirror and propagate again through the converter. On return, we must recover a Langmuir wave of amplitude unity and no

transverse wave since the system is non dissipative

$$1 = |R_L| \exp(-i r_L)\ |R_L| \exp(i r_L) + |T_T| \exp(-i t_T) |T_L| \exp(i t_T),$$

$$0 = |R_L| \exp(-i r_L)\, |T_T| \exp(i t_T) + |T_T| \exp(-i t_T) |R_T| \exp(i r_T).$$

From the latter relation follows $|R_L| = |R_T|$, $r_L + r_T = 2\, t_T - \pi$, and from the former follows $|T_T|\ |T_L| = 1 - |R_L|^2$, $t_L = t_T$. Thus by virtue of the previous equivalences the reciprocity principle is proved.

For conversion, our computation showed that only the vicinity of the critical point $X_o$ is of importance. Thus the effect of density profile may be accounted for, in many cases, by a tangential approximation of the slope near $X_o$. Due to this fact, the curve A(q) (cf. Fig. 2) takes a character quasi universal. It allows us to give the absorption for the TL problem as well as for the LT problem in view of the reciprocity principle. Moreover, the emission coefficients may themselves be derived from it as we shall see.

## 2. Effect of the external force

We have already mentioned the difference existing between the emission and the corresponding absorption coefficient. The energy absorbed from one type of waves differs from the energy emitted into the other type even in a non-dissipative medium. Now, since $\varepsilon_L^T \, \varepsilon_T^L = A^2$ by the reciprocity principle, the sign of the difference changes between the LT and the TL problem. The external force gives some energy to the wave in the case of the LT problem and extracts it from the wave in the TL problem. Within the WKB approximation this feature may be interpreted in a consistent manner with the change in the direction of propagation of the Langmuir wave that distinguishes one problem from the other. Then the external force that is hidden in the $\alpha$-term in Eq. (3) would act on the Langmuir wave exclusively.

On the other hand the flux of energy associated with the propagation of a Langmuir wave in a density gradient is not conserved, Eq. (20).

$$S_x^L(x) = \frac{3\beta c^2}{8\pi\omega} \frac{k_y^2 + k_L^2(x)}{k_L(x)} \left| E_x^{(0)} \right|^2 ,$$

$$\text{where} \quad E_x^{(0)} = \left[ \frac{c^2 k_L(x) n(x)}{\omega^2 - \omega_p^2(x)} \right]^{1/2}$$

is the lowest order term of the WKB solution of Eqs. (3) and (4). Hence the Langmuir flux scales like

$$S_x^L(x) \sim \frac{h(x)}{\omega} .$$

By using this property, we may derive straightforwardly a formula for the emission coefficient that agrees well with the numerical calculations

$$\mathcal{E}_T^L = A_T^L \frac{q(0)}{1 - \mathcal{H}_c (x_0 - x_L)} \simeq A_T^L \; q(0) \qquad (33),$$

where $x_0$ is the critical point, $x_L$ the turning point for Langmuir waves, and $\mathcal{H}_c = \mathcal{H}(x = x_0)$.

Thus, all our numerical results concerning the absorption and emission of high-frequency waves due to a density gradient may be approximately recovered by means of a unique curve A(q), Fig. (2). As long as the temperature is not too high (under 50 keV) the role of the parameter $\beta$ may be ignored with respect to the four absorption and emission coefficients $A_L^T$, $A_T^L$, $\varepsilon_L^T$ and $\varepsilon_T^L$.

## III. ELECTROMAGNETIC RADIATION FROM AN INHOMOGENEOUS PLASMA

Even in a stable plasma there exists a finite level of plasma waves. Those are normal modes of the system and represent degrees of freedom which are excited in thermal equilibrium. Plasma waves are emitted by particles as they move about in the plasma, and they are absorbed again by the plasma, for example, via collisions or via Landau damping. The balance between emission and absorption leads to a thermal level of field fluctuations. It may be imagined that some of the Langmuir waves present are converted into electromagnetic radiation if there is a density gradient. In this section, we shall try to develop this idea in order to obtain the spectrum of the radiation emitted in the $\omega_{pe}$ range by a gradient of density in a plasma.

Let us assume that a population of plasmons coexists with the plasma particles. The population is assumed to be in an equilibrium characterized by an effective temperature $T_{eff}$, which may be different from the electron temperatue $T_e$. This assumption is essential for introducing the statistic of the number of plasmons.

Let us consider plasmons with a given frequency $\omega$ and direction $(\Theta_L, \phi)$ where $\Theta_L$ is the pitch-angle and $\phi$ the azimuthal angle with resepct to the gradient. The number of states is equal to

$$\delta N_K^L = \frac{1}{(2\pi)^3} k_L^2 \delta k_L \sin\theta_L \delta\theta_L \delta\phi \quad \text{per cm}^3 \tag{34}.$$

Here $k_L$ is related to $\omega$ by the local relation

$$k_L(x) = \frac{\omega}{(3\beta)^{1/2} c} \left[1 - g(x)\right]^{1/2} \tag{35}.$$

Thus the number of states varies along the ray, which seems cumbersome at first sight. However, it turns out that the corresponding elementary Poynting flux

$$\delta S_K^L = T_{eff} \cdot v_g \cdot \delta N_K^L \tag{36}$$

is conserved along the ray due to the behavior of the group velocity $v_g$.

The conservation of the Poynting flux along the ray suggests a model (Fig. 4) where the statistic of the plasmons is calculated in the homogeneous part ($X < 0$) even if the plasmons that are really converted do not originate from there. Simply stated the rays establish a virtual link between the plasmons which appear in the statistics and those which are converted. Thus, there is a unique relation between the frequency and the solid angle appearing in the spectrum of emission, and the degrees of freedom invoked in the statistics.

By applying the LT conversion on the Poynting flux

$$\delta S_k^L = T_{eff} \frac{1}{(2\pi)^3} 3 v_e^2 \frac{k_L^3}{\omega} \delta k_L \sin\theta_L \delta\theta_L \delta\phi ,$$

we find

$$\delta S_k^T = T_{eff} \frac{A(q)}{(2\pi)^3} \frac{c^2}{\omega} k_T^3 \delta k_T \sin\theta_T \delta\phi \, \delta\theta_T ,$$

or, expressed in frequency

$$\delta S_\omega^T = T_{eff} \frac{A(q)}{(2\pi)^3} (1 - q_0) \frac{\omega^2}{c^2} \delta\omega \sin\theta_T \delta\theta_T \delta\phi \qquad (37),$$

where A is evaluated for the values of q corresponding to the angle and frequency chosen. Then, an intensity may be defined

$$I_\omega(\theta) = \frac{T_{eff}}{(2\pi)^3} A\left[q = \left(\frac{\omega_{p_0} L}{c}\right)^{2/3} \sin^2\theta \left(\frac{\omega^2}{\omega_{p_0}^2} - 1\right)\right] \frac{\omega^2 - \omega_{p_0}^2}{c^2} \qquad (38).$$

This formula looks similar to the Rayleigh-Jeans law even though the plasma is optically thin. It should be emphasized that the statistical part of the formula refers to plasmons; for them the plasma is opaque and a thermal level may be reached. However, the linear conversion constitutes a tunnel between the plasmon domain and the photon domain; thus a radiation intensity of the order of the black body radiation may be emitted by a transparent plasma with a density gradient for some angles and frequencies.

## IV. EXPERIMENTAL RESULTS

The experiment on linear conversion was performed in a large d.c. discharge Argon plasma.[18] The chamber is shown in Fig. 5. The diameter of the cylindrical plasma is 180 cm and the length is 320 cm. These dimensions are much larger than the vacuum wavelength for the 2 GHz band. Tungsten filaments are distributed around the walls in four separate groups. Each group of filaments can be heated and biased separately, and, since the mean free path of an ionizing electron is approximately 100 cm, a density gradient can be maintained by controlling the discharge current from each group. A microwave horn antenna is immersed in the plasma at one end of the machine for observing the radiation. Moveable Langmuir probes can measure the plasma electron temperature and density both axially and radially. These probes are always withdrawn from the plasma when the radiation is measured. A typical axial density profile is shown in Fig. 6. The density varies from $2.0 \cdot 10^{10}/cm^3$ to $5.3 \cdot 10^{10}/cm^3$. The electron temperature is constant at 1.4 eV and the ion temperature is typical of this weakly ionized plasma at approximately 0.2 eV. The radial density profile is shown in Fig. 6. The density is seen to be constant within 10% out to a radius of 70 cm.

A block diagram of the experiment is shown in Fig. 7. The preselector is a narrow band tunable filter which tracks the frequency of the spectrum analyzer and eliminates intermodulation signals generated in the amplifier. The noise level of the system for a 300 kHz bandwidth was $10^{-14}$ Watts at 1.8 GHz. The frequency response of the amplifier

fell considerably above 2.1 GHz and the microwave horn had a cut-off below 1.5 GHz. Thus the spectrum of the radiation emitted by the plasma can be compared with the spectrum predicted by the linear conversion theory presented in Section III.

The axial density profile was measured automatically by a microprocessor connected to a Langmuir probe. The microprocessor controlled the position of the probe and measured its current versus voltage characteristic. It then reduced the data and printed out the density, electron temperature, plasma potential and position every 5 cm along the axis of the chamber. This was done every time the density profile was changed (by varying the emission currents) and a new emission spectrum was recorded. The emission spectrum was always measured in presence of primary ionizing electrons. Measurements in an afterglow plasma will be discussed in connection with the role of primary electron: in such configuration, the electromagnetic level is equal to the bremsstrahlung level.

In our experimental device, microwave reflection on the wall, though inevitable, does not affect the measurements. This observation is supported by the following. In a previous experiment,[19] where an incident microwave beam was launched onto a density gradient, the characteristic Airy pattern was observed. Would the wall reflection be important, this pattern would be destroyed. Secondly, the machine is in no sense a high Q cavity. Around four hundred stainless steel filaments supports

(10 cm long) protrude inside the plasma, giving rise to a structure similar to the "microwave absorber forest" described recently by d'Angelo et al.[20]

The linear conversion model presented in Section III did not take into account the radiation pattern of the receiving antenna. In order to calculate the power received by the microwave horn one must multiply the intensity given by Eq. (38), by an antenna gain function and integrate over all solid angles

$$P_\omega = \int d\Omega \; I_\omega(\theta) \, G(\theta, \phi) \tag{39}$$

The antenna gain function is only approximately known. It can be calculated[21] by assuming that it is the pattern given by a rectangular waveguide in the $TE_{01}$ mode. This is a commonly-used good approxima-

tion and the antenna pattern in the E plane for a wavelength of 15 cm is shown in Fig. 8. However, the antenna pattern must be modified to take into account diffraction of the wave in the presence of the plasma density gradient.

Consider an electromagnetic wave which leaves the antenna at an angle, $\Theta$, with a frequency, $\omega$, corresponding to an $\omega_p$ at a particular layer in the plasma. This is shown schematically in Fig. 9. There is a possibility that this wave will never reach the critical layer since the plasma has a finite radius. The maximum angle, $\Theta$, which allows the ray to remain inside the chamber and still reach its critical layer must be calculated for each frequency and density profile and then inserted as a limit in the integral over the antenna function. The cutoff angle calculated for the density profile shown in Fig. 6 is shown in Fig. 10. To be consistent with the use of the far field gain expression of the antenna, an additional cutoff angle, $\alpha_c = 60^\circ$, was imposed. This angle is arbitrarily defined as

$$\alpha_c = \text{Arc tan} \frac{\text{Radius of the plasma}}{\text{Largest size of the antenna}}$$

which yields in our case Arc tan (.6/.3) or approximately $60^\circ$. Furthermore, Fig. 8 shows that the antenna gain is small for $\alpha$ greater than $40^\circ$ so that uncertainties in $\alpha$ will not affect the result.

The power spectrum calculated from Eq. (39) for the horn antenna used in the experiments and for the density profile shown in Fig. 6 is shown in Fig. 11. The plasmon spectrum was assumed to be thermal, e.i., $W_k = T_e$. The vertical scale is in dB with respect to one milliwatt (-100 dBm = $10^{-10}$ mW). The power spectrum measured in the experiment is shown in Fig. 12. The shapes of the two spectra are similar, but the received power in the experiment is approximately three order of magnitude higher than the power emitted by the thermal plasmon spectrum.

For the moment, one can ignore the three orders of magnitude difference and investigate the functional dependence of the spectrum on the density profile. A series of experiments was performed in which the density of the plasma at the antenna was kept constant at 2.0 $10^{10}/cm^3$. The axial location of the peak density was also kept fixed. The only variable was the peak density. This density profile can be modelled by the equation

$$n(x) = n_o + \Delta n \sin\left(\frac{\pi x}{2L}\right) \qquad (40),$$

where $n_o$ is the density at the antenna, $\Delta n$ is the difference between $n_o$ and the peak density and L is the location of the maximum density measured from the antenna.

The results of this series of experiments are shown in Fig. 13. The maximum of the power spectrum is plotted vs $\Delta n$. The dots are the experimental points with experimental error bars attached and the solid line is the result calculated from our model. The theoretical curve has been scaled up 30 dB in this case. As expected, when the density profile was flattened, the radiation decreased. When the profile was very flat ($\Delta n \lesssim 0.2 \cdot 10^{10}$), only a weak radiation (-105 dBm) with no peak was seen. This was attributed to bremsstrahlung and is discussed later. The functional characteristics of the model agree very well with the experiment over a range of more than two orders of magnitude in power.

Another set of experiments was performed in which $n_o$ and $\Delta n$ were kept constant and L was varied. The results of this series is shown in Fig. 14. The maximum of the power spectrum was plotted as a function of L. Again the solid line is calculated from the model (rescaled 30 dB) and the circles are the experimental values. The peak power is only a weak function of L according to the model and this is seen experimentally.

The presence of a radial density gradient does not affect these results. Conversion of either Langmuir wave or other types of waves (upper hybrid for example) would yield an EM wave propagating towards the wall, and would not be received by the horn. On the other hand, the power emitted from the plasma is greatly reduced when the axial gradient is diminished (Fig. 13 and 14). The radial density gradient, however, is not

affected by the variation of the axial density gradient: if the radiation is due to the radial density gradient, then its level would not be affected when the axial density gradient is changed, which is not the case.

Thus the radiation obeys the laws of our model of linear conversion. We have, however, had to assume an enhanced level of plasmons. Let us, as an alternative, consider bremsstrahlung as a possible source of the radiation.

The emission from an optically thin plasma[22] is given by

$$j_\omega = \frac{n_e n_i Z^2 e^6}{48 \pi^4 \varepsilon_0^3 c^3 m^2} \left(\frac{m}{2\pi k_B T}\right)^{1/2} \times \ln\left[1.336 \left(\frac{k_B T}{m}\right)^{3/2} \frac{4\pi \varepsilon_0 m}{Z e^2 \omega}\right] \qquad (41).$$

The units are MKS. This emission $j_\omega$ has units of watts meter$^{-3}$ steradian$^{-1}$ (radian sec$^{-1}$)$^{-1}$. It can be used as a source term in Eq. (39) and a received power spectrum for a plasma with the density profile shown in Fig. 6 can be calculated. This Bremsstrahlung radiation is shown in Fig. 15. Its level is lower than that predicted by the linear conversion of a thermal plasmon spectrum and thus cannot be the source of the enhanced radiation. For a non-Maxwellian plasma, however, the Bremsstrahlung itself can be enhanced. A recent review article by Papadopoulos and Freund discusses this point in more detail.[23]

For a two temperature plasma, the distribution function is given by

$$f(v) = \frac{\delta}{(2\pi)^{3/2} v_e^3} \left[ \exp\left(-\frac{v^2}{2 v_e^2}\right) + (1-\delta)\frac{v_e^2}{v_E^2} \exp\left(-\frac{v^2}{2 v_E^2}\right) \right] \quad (42),$$

where $v_E$ is the high temperature thermal velocity, $v_e$ is the low temperature thermal velocity, and $\delta$ is the percentage of the low temperature plasma.

There is an enhanced emission by the factor

$$F = \frac{v_E^2 / v_e^2}{\ln\left[\frac{v_E}{v_E (1-\delta)}\right]} \quad (43).$$

For the experimental plasma the ionizing electrons have an energy of 60 Volts and a concentration such that $1-\delta \tilde{\sim} 10^{-4}$. Thus F = 5.3. Even a high temperature component density of $10^{-3}$ gives only an enhanced factor of 6.7. This is clearly too small to explain the observed enhancement factor of 1000. Furthermore, if the observed radiation were due to bremsstrahlung, the level would not drop by 30 dB as a constant density profile was approached. Thus the enhanced plasmon level remains as the probable source of the radiation.

The ionizing electrons come off the filaments which are uniformly distributed around the walls of the chamber. The corresponding beams with a radial velocity component overstep the large density gradient near the boundaries of the plasma (cf. Fig. 6). They do not relaxe quasilinearly because of the lack of synchronisation between the waves and the beam particles (Ref. 24, p. 18), but penetrate into the nearly constant density region ($r < 60$ cm) with a velocity spread $\Delta v \gtrsim 1\ v_e$ around the velocity $v_b = \left(\frac{60}{1.4}\right)^{\frac{1}{2}} v_e = 6\ v_e$. There, these beams cause an instability that enhances the plasma level. However, since they are multidirectional and come from different sources distributed around, they may interact with each other through the waves excited. Their dynamics of relaxation is thus far from being a trivial problem and beyond the scope of this paper if any. Therefore, we resort to a rough estimation of the relaxation length and the energy density of the plasmons from simple considerations. A typical group of filaments has a 10 A discharge spread over an area $A = 2\pi RL$, where $R = 90$ cm and $L = 75$ cm. Thus the density of ionizing electrons is $n_i = I/(AeV_b)$. Since these electrons constitute many beams, the average density per beam may be estimated as $\xi_b = n_i/2\pi$. For $v_b = 6\ v_e$ one obtains $\xi_b = 7.3\ 10^5$ and, for $n_o = 3\ 10^{10}\ cm^{-3}$ and $T = 1.4$ eV, plasma waves grow with a rate $\gamma \approx \omega_p (\xi_b/n_o)\ (v_b/\Delta v)^2 = 1.8\ 10^7$ rad/sec $>> \nu_o = 10^6$ rad/sec, where $\nu_o$ is the collision frequency. The beam is not relaxed over a length shorter than $l_{\frac{1}{2}} = 0.2(n_o/\xi_b)\ (v_e^2/\omega_p v_b)\Lambda \approx 70$ cm (Ref. 24, p. 10) so that the plasmon level is enhanced everywhere till the center of the plasma. Since the plasmon energy density produced by a beam is (Ref. 24, p. 10) $W_b = \xi_b\ mv_b^4/15\ v_e^2$, we may estimate the total energy density as a sum

over all beams, namely $W = 2\pi W_b$, which leads to an enhancement factor on the thermal level $W_{th} = T/6\pi^2\lambda_D^3$ of

$$F = \frac{W}{W_{th}} \approx \pi^3 \lambda_D^3 \left\{_b \left(\frac{v_b}{v_e}\right)^4 \right. \tag{44}$$

For the values of the parameters indicated one obtains F = 3700 that is approximately the factor of 1000 needed. However, this factor is overestimated since it does not take into account possible losses, starting with the ionizing collisions the mean-free path of which $\tilde{\sim}$ 100 cm is not far from the relaxation length $l_{\frac{1}{2}} \tilde{\sim}$ 70 cm. A further point we have to assume is that, due to the multidirectionality of the beams, plasma waves with all sorts of $\vec{k}$ are excited so that F is the enhancement factor above the thermal level for each degree of freedom. This strong assumption is at least not contradictory with the experimental fact that the noise power is constant along a radius for r < 60 cm.

Also, we have considered the possibility of an enhanced plasmon level due to spontaneous processes (Čerenkov and longitudinal bremsstrahlung) associated with a non maxwellian distribution of electrons. However, we found the enhancement to be negligible; typically F = 1-5.

Experimentally the influence of the ionizing electrons was investigated by switching off the voltage on the filaments and working in the afterglow plasma. The switch-off time is approximately 10 μsec. The density of the plasma changes on the time scale of milliseconds.

It was seen that the radiation level fell to approximately -105 dBm, in a time of 10 μsec, long before the density profile changed (Fig. 16). Thus the source of the enhanced radiation is experimentally demonstrated to be the primary electrons.

It is difficult to directly measure the plasmons themselves locally by means of probes at these frequencies. A probe cannot easily distinguish between an electrostatic wave and an electromagnetic wave and, furthermore, the coupling constant for each of these is unknown and varies considerably with frequency above several hundred MHz. The probe itself can also disturb the plasma.

## V. CONCLUSION

We have studied theoretically and numerically the linear conversion of a Langmuir wave into a transverse wave in a field-free inhomogeneous plasma. The emission and absorption coefficients ($\varepsilon_L^T$ and $A_L^T$) due to the LT conversion can be deduced from the emission and absorption coefficients ($\varepsilon_T^L$ and $A_T^L$) due to the TL conversion. This general principle has been proved both theoretically and numerically. The

emission of electromagnetic waves from a stable inhomogeneous plasma has then been computed. In the calculations, an equilibrium state for the plasmons has been assumed. In order to be able to compare it with the experimental result, we also introduced the gain function of the antenna used in the experiments. Aside from a discrepancy in the absolute amplitude, main features predicted by the theory, such as dependency of the emitted power upon the density gradient characteristics, were verified experimentally. The discrepancy in the absolute amplitude was due to the ionizing electron beam which excited a non-thermal level of plasmons.

ACKNOWLEDGMENTS

We would like to thank Dr. K. Appert and Prof. C.S. Liu for fruitful discussions. This work was partially funded by the Swiss National Science Foundation and Euratom.

REFERENCES

{1} V.L. Ginzburg, Propagation of Electromagnetic waves in Plasmas (Pergamon Press, New York, 1970) 2nd edition, p. 261 and following.

{2} D.W. Forslund, J.M. Kindel, K. Lee, E.L. Lindman, and R.L. Morse, Phys. Rev. A. 11, 679 (1975).

{3} A.D. Pilya, Zh. Tekh. Fiz. 36, 818 (1966) [Sov. Phys. Techn. Phys. 11, 609 (1966)].

{4} J.P. Freidberg, R.W. Mitchell, R.L. Morse, and L. I. Rudsinski, Phys. Rev. Lett. 28, 795 (1972).

{5} N.G. Denisov, Zh. Eksp. Teor. Fiz. 31, 609 (1956) [Sov. Phys. JETP 4, 544 (1957)].

{6} R.P. Godwin, Phys. Rev. Lett. 28, 85 (1972).

{7} K.G. Budden, Radio Waves in the Ionosphere, (Cambridge U.P., Cambridge, England, 1961), p. 348 and followings.

{8} R.B. White and F.F. Chen, Plasma Phys. 16, 565 (1974).

{9} D.A. Tidman, Phys. Rev. 117, 336 (1960).

{10} R. Stenzel, A.Y. Wong and H.C. Kim, Phys. Rev. Lett. 32, 654 (1974).

{11} K. Adati, H. Iguchi, Y. Ito, and T. Kawabe, Plasma Physics 19, 167 (1977).

{12} P. Brossier, A.E. Costley, D.S. Komm, G. Ramponi, and S. Tamer in Plasma Physics and Controlled Nuclear Fusion Research (International Atomic Energy Agency, Vienna, 1977), Vol. I, p. 409.

{13} I. Fidone, G. Ramponi, and P. Brossier, Phys. Fluids 21, 237 (1978).

{14} A.E. Costley in Proceedings of the International Conference on Synchrotron and Runaway Electrons in Tokamaks (University of Maryland, College Park, Md., 1977), Paper B3.

{15} I.H. Hutchinson and D.S. Komm, Nucl. Fusion 17, 1077 (1977).

{16} I.H. Hutchinson and S.E. Kessel, Phys. Fluids 23, 1698 (1980).

{17} G. Strange and G.J. Fix in An Analysis of Finite Element Method (Prentice-Hall, Engelwood Cliff, N.J., 1973), p. 24.

{18} R. Limpacher and H.R. McKenzie, Rev. Sc. Instrum. 44, 726 (1973).

{19} R.W. Means, V.P. Silin, and M.Q. Tran, Pis'ma Zh. Ehsp. Teor. Fiz 29, 154 (1979) (JETP Lett. 29, 137 (1979)).

{20} M.J. Alport, N. d'Angelo, and M. Khazei, IEEE Trans. Plasma Sciences, PJ 8, 111 (1980).

{21} L.J. Chu, J. Appl. Phys. 11, 603 (1940), reprinted in Electromagnetic Horn Antennas, edited by A.W. Lowe (IEEE Press, New York, 1976), p. 38.

{22} G. Bekefi, Radiation Processes in Plasmas, p. 87, 1966, Wiley.

{23} K. Papadopoulos and H.P. Freund, Space Science Reviews 24 511-566, (1979).

{24} A.A. Vedenov and D.D. Ryutov, in Reviews of Plasma Physics, edited by M.A. Leontovich (Consultants Bureau, New York, 1975), Vol. 6.

## FIGURE CAPTIONS

Figure 1 — Model of plasma density profile. For $X < 0$, a constant density is assumed. We also represent schematically the propagation of a transverse wave (∿∿) and of a Langmuir wave (wwww). $X_T$, $X_L$ are respectively the reflection points of the transverse, Langmuir wave. $x_o$ is the critical point.

Figure 2 — Variation of $A = A(q)$.

Figure 3 — Cycle used to demonstrate the reciprocity principle.

Figure 4 — Sketch of the model used in the computation of the electromagnetic emission from an inhomogeneous plasma.

Figure 5 — The experimental device. The size of the plasma volume is 3m length and 2m diameter. A pyramidal horn is used to detect the electromagnetic wave. Longitudinal and radial probes controlled by a microprocessor allow to measure the density profile.

Figure captions (cont'd)

Figure 6 Typical axial and radial density profile.

Figure 7 Block diagram of the microwave detection system.

Figure 8 Normalized antenna gain as a function of the angle.

Figure 9 Schematic representation of the ray of an electromagnetic wave as it propagates down the gradient. A ray which will reach the horn at an angle greater than $\Theta$ would be generated outside the plasma radius and therefore would not exist.

Figure 10 Variation of the cutoff angle.

Figure 11 Computed frequency spectrum of the transverse wave emitted by the plasma. The density gradient is shown in figure 7.

Figure 12 Measured frequency spectrum of the transverse wave emitted by the plasma. The density gradient is shown in figure 7. Note that the level is higher by 30 db compared to the computed one (Fig. 12).

Figure 13 Variation of the maximum level of the frequency spectrum with the density gradient amplitude $\Delta n$. Dots ( ● ) are experimental points. The square ( ■ ) is the level measured for a flat profile. The solved curve is the rescaled theo-

Figure captions (cont'd)

Figure 13 (cont'd)

retical values computed assuming a profile $n(X) = n_o + \Delta n \sin\pi X/L$ with $n_o = 2 \cdot 10^{10}$ cm$^{-3}$ and L = 120 cm.

Figure 14 Variation of the maximum level of the frequency spectrum with the gradient scale length L. The solid curve is the rescaled theoretical prediction. The density profile is $n(X) = n_o + \Delta n \sin\pi X/L$ where $n_o = 3 \cdot 10^{10}$ cm$^{-3}$ et $\Delta n = 1.5 \cdot 10^{10}$ cm$^{-3}$.

Figure 15 Computed Bremsstrahlung spectrum for an inhomogeneous plasma. Both the density profile of Fig. 7 and the antenna gain function were included in the calculation.

Figure 16 Time evolution of the emitted electromagnetic wave and the plasma density. The arrow indicates the time where the primary electrons are switched off. Note the rapid decay of the electromagnetic wave, while in the same time the density remains constant.

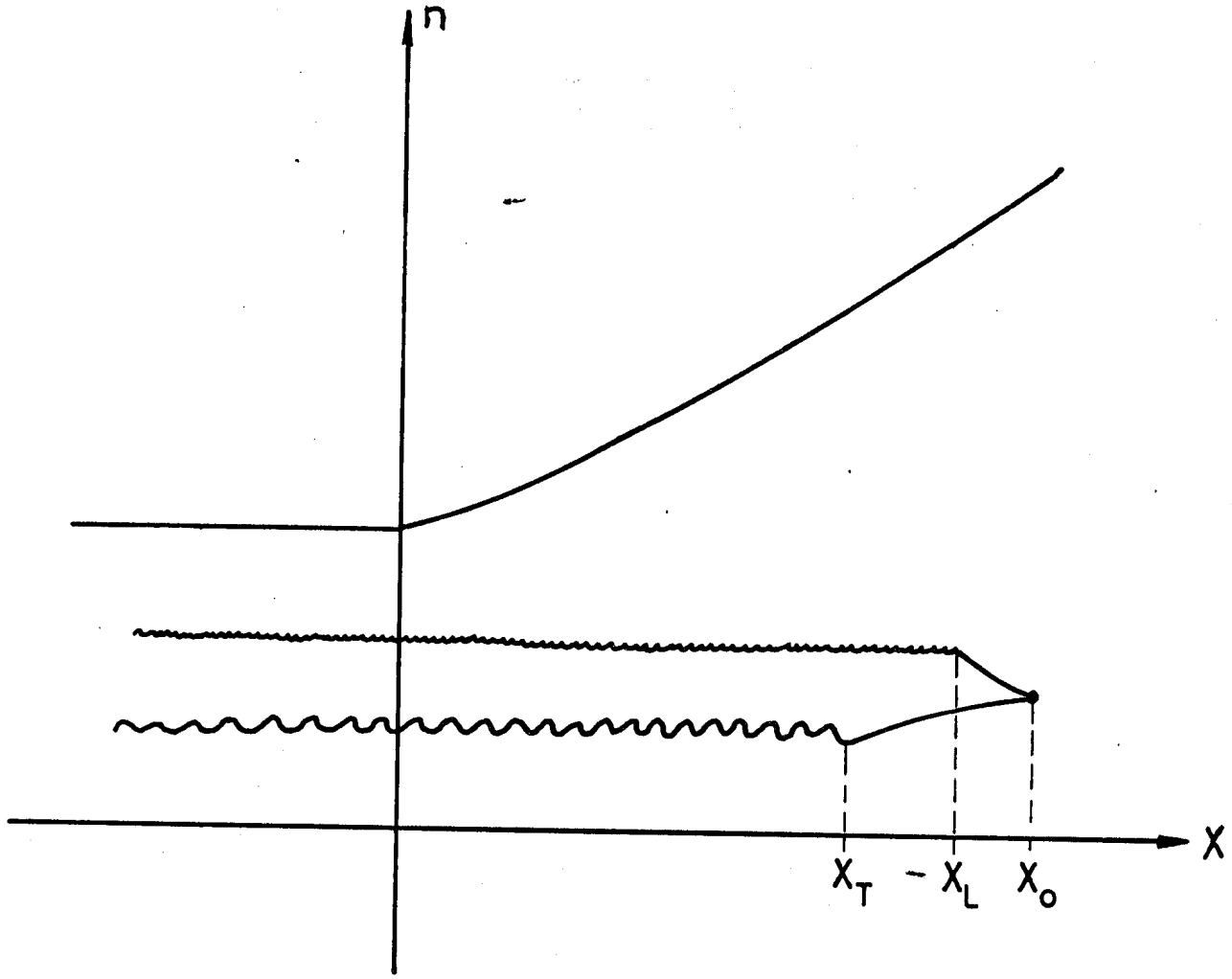


Fig. 1

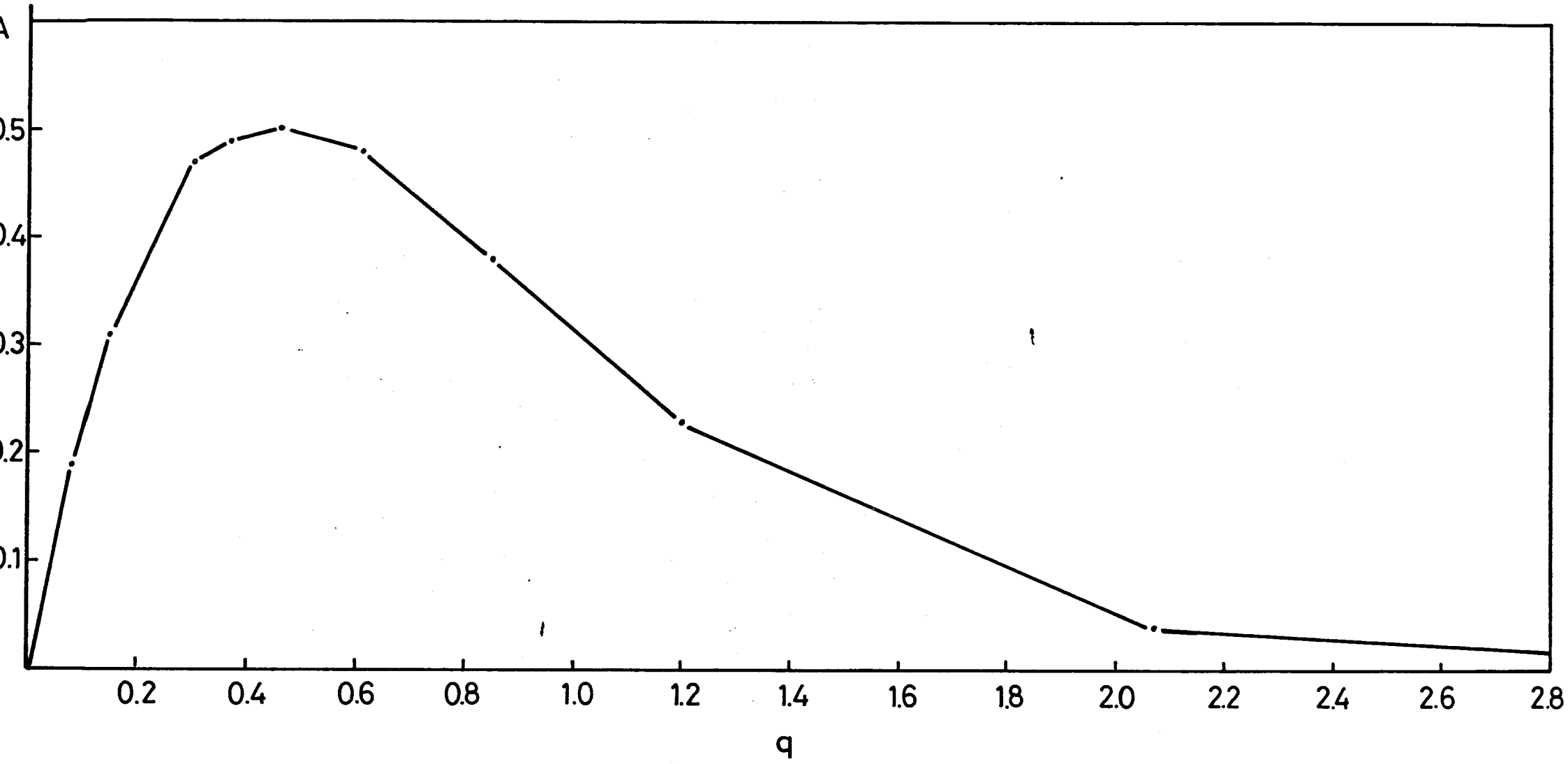


Fig. 2

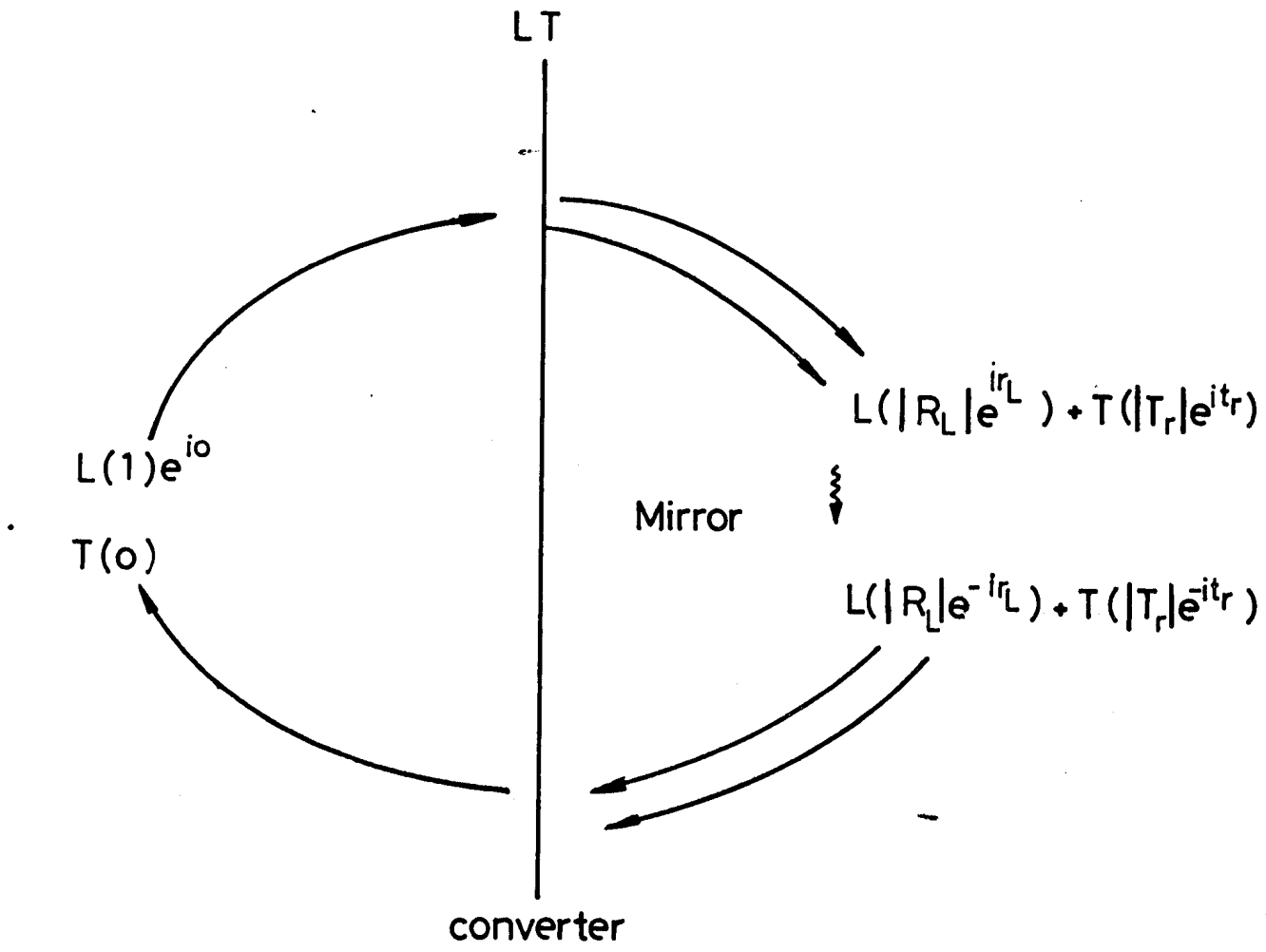
LT
L(1)e^{io}
T(o)
L(|R_L|e^{ir_L}) + T(|T_r|e^{it_r})
Mirror
L(|R_L|e^{-ir_L}) + T(|T_r|e^{-it_r})
converter

Fig. 3

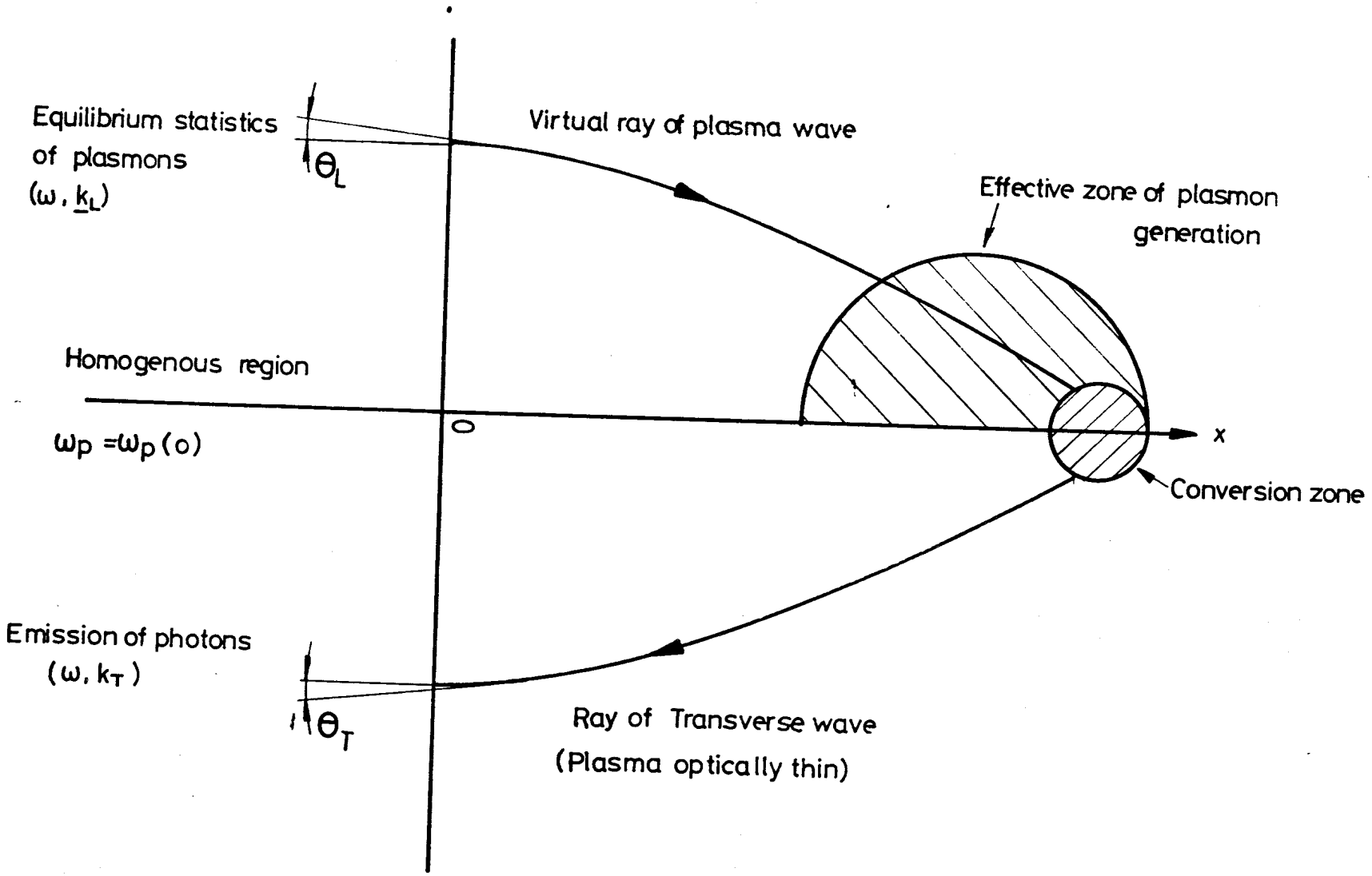
Equilibrium statistics
of plasmons
$(\omega, \underline{k}_L)$
$\theta_L$
Virtual ray of plasma wave
Effective zone of plasmon
generation
Homogenous region
$\omega_p = \omega_p(o)$
o
x
Conversion zone
Emission of photons
$(\omega, k_T)$
$\theta_T$
Ray of Transverse wave
(Plasma optically thin)

Fig. 4

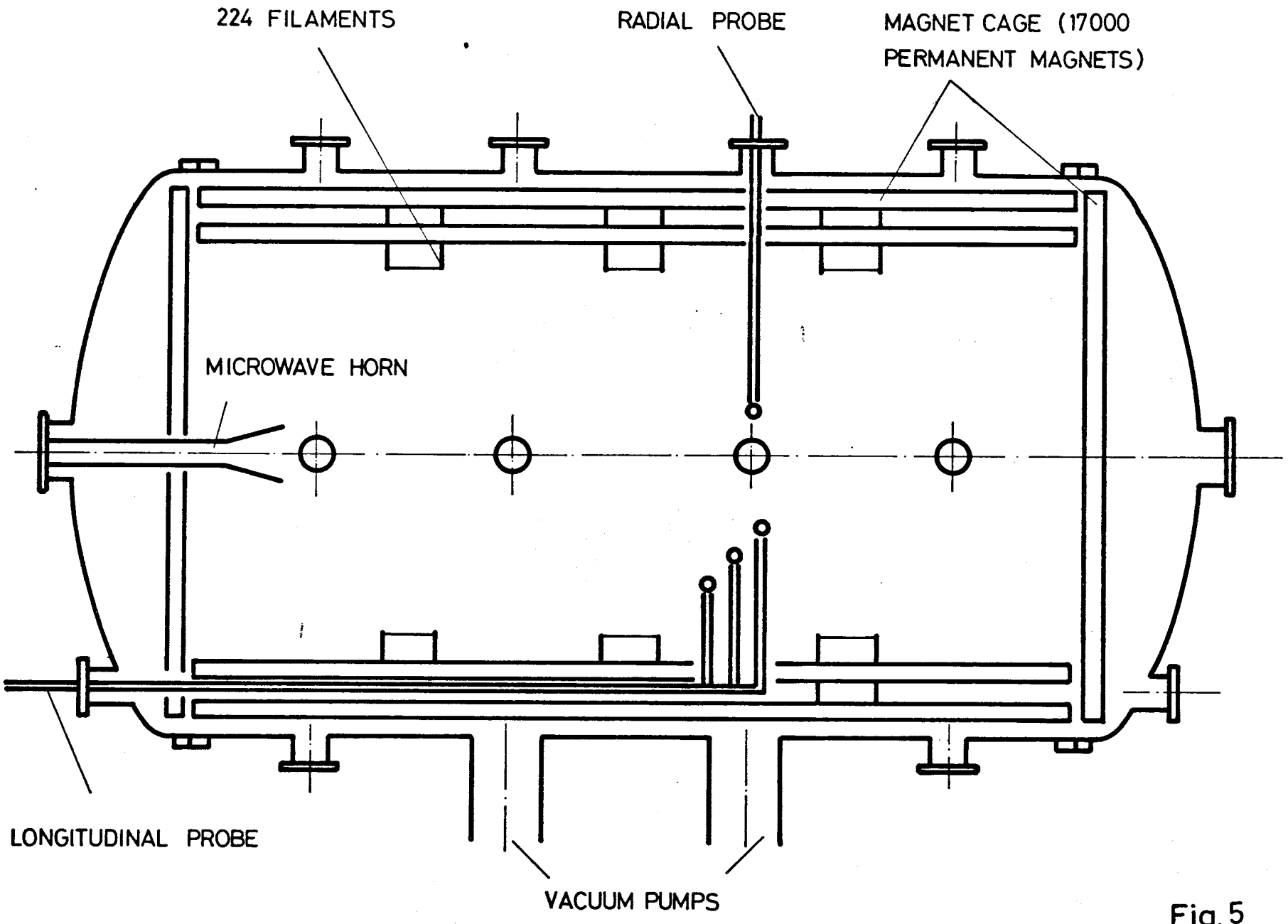
224 FILAMENTS
RADIAL PROBE
MAGNET CAGE (17000
PERMANENT MAGNETS)
MICROWAVE HORN
LONGITUDINAL PROBE
VACUUM PUMPS

Fig. 5

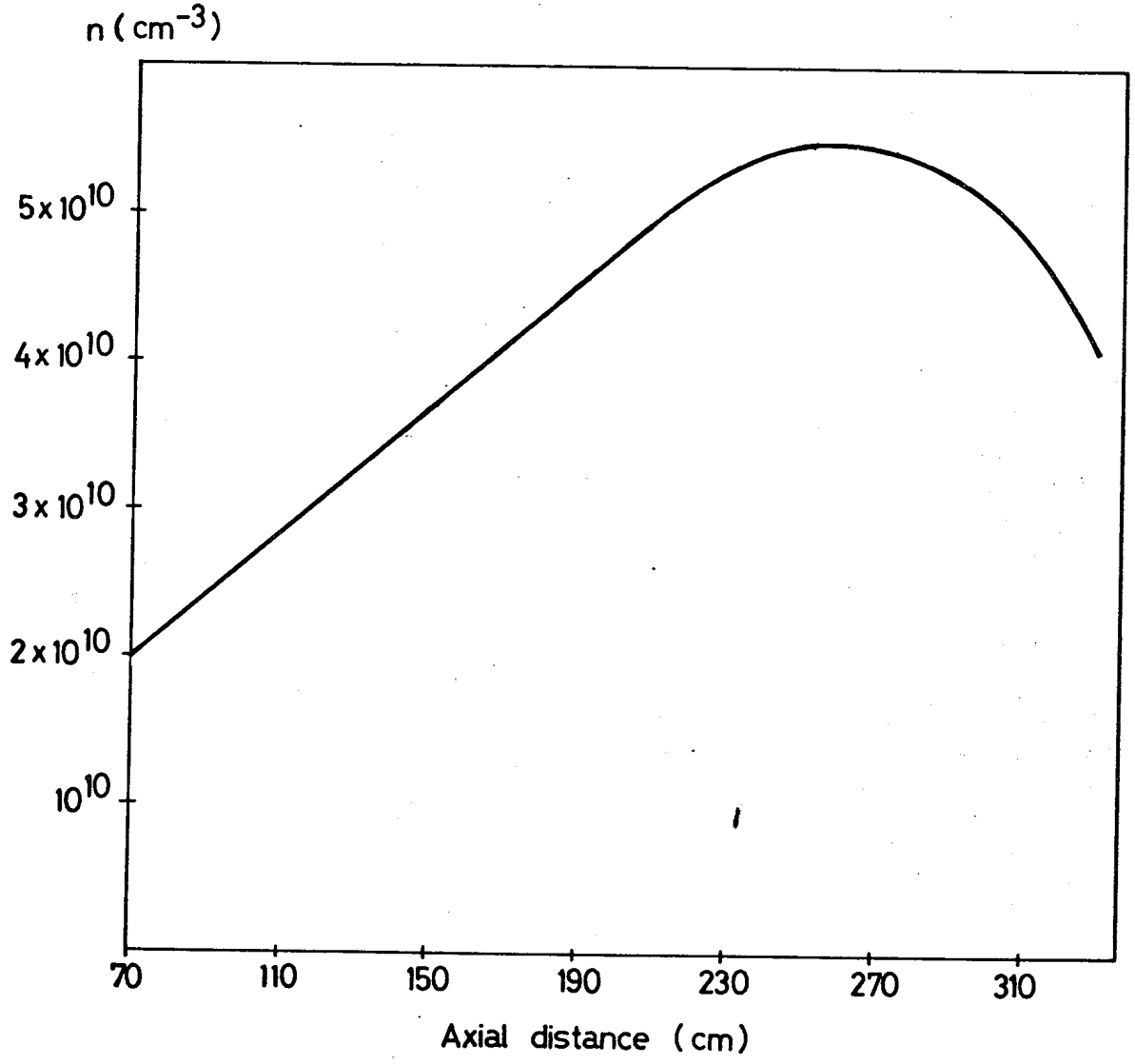
n ( cm$^{-3}$)
5x10$^{10}$
4x10$^{10}$
3x10$^{10}$
2x10$^{10}$
10$^{10}$
70
110
150
190
230
270
310
Axial distance ( cm)

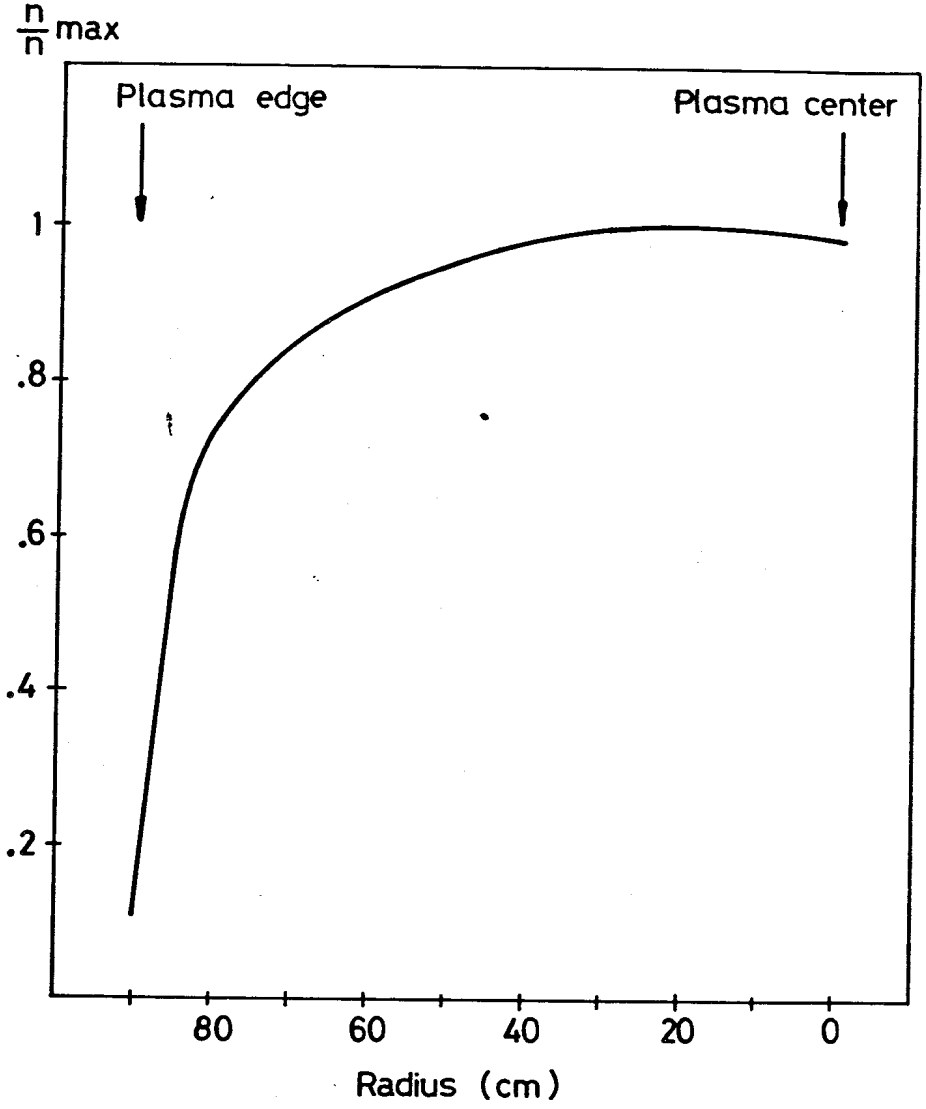
n/n max
Plasma edge
Plasma center
1
.8
.6
.4
.2
80
60
40
20
0
Radius (cm)

Fig.6

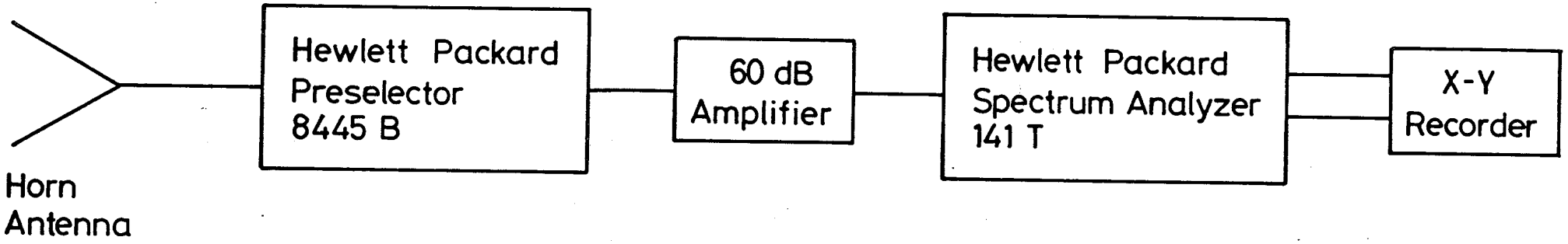
Horn
Antenna
Hewlett Packard
Preselector
8445 B
60 dB
Amplifier
Hewlett Packard
Spectrum Analyzer
141 T
X-Y
Recorder

Fig. 7

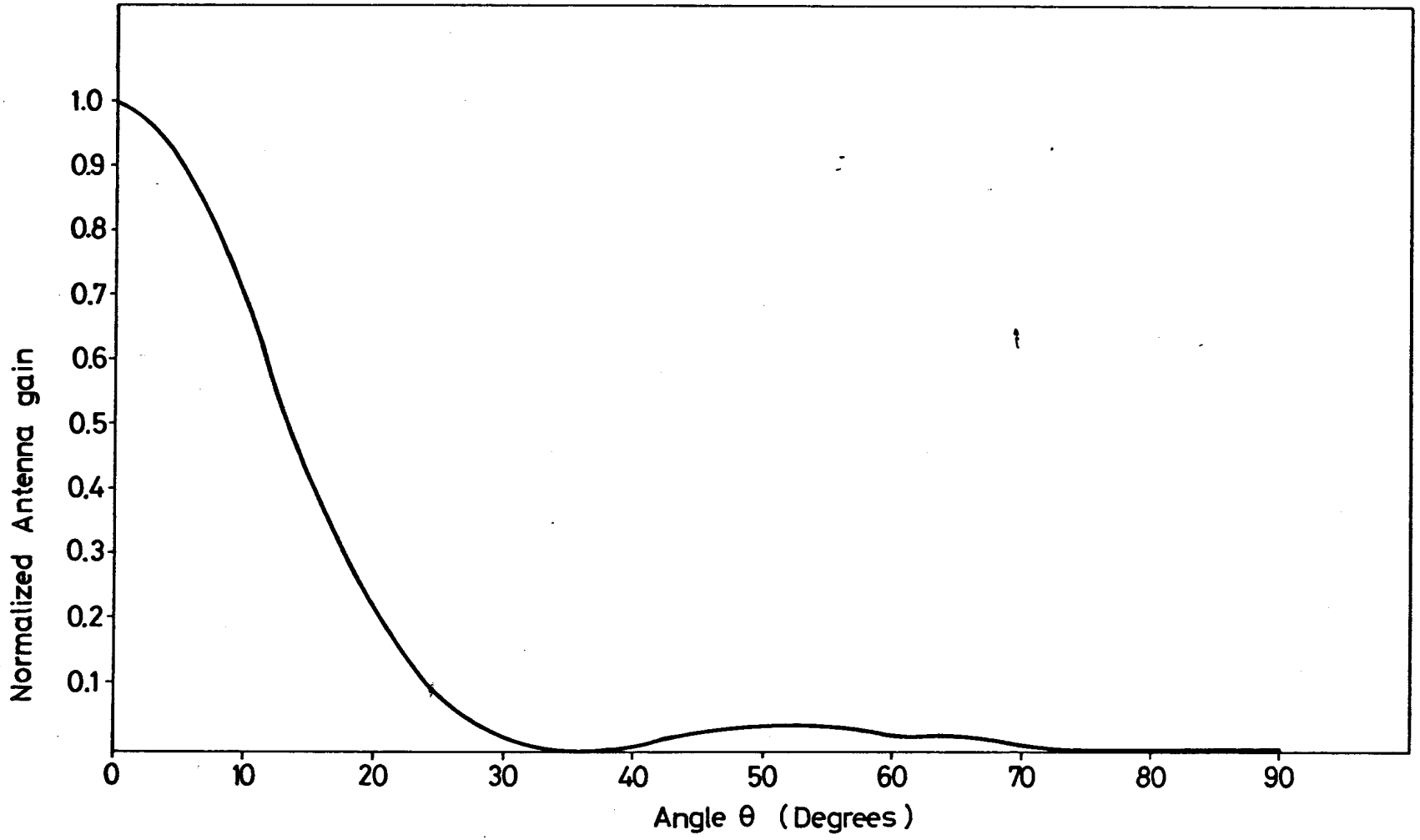
Normalized Antenna gain
1.0
0.9
0.8
0.7
0.6
0.5
0.4
0.3
0.2
0.1
0
10
20
30
40
50
60
70
80
90
Angle θ (Degrees)

Fig.8

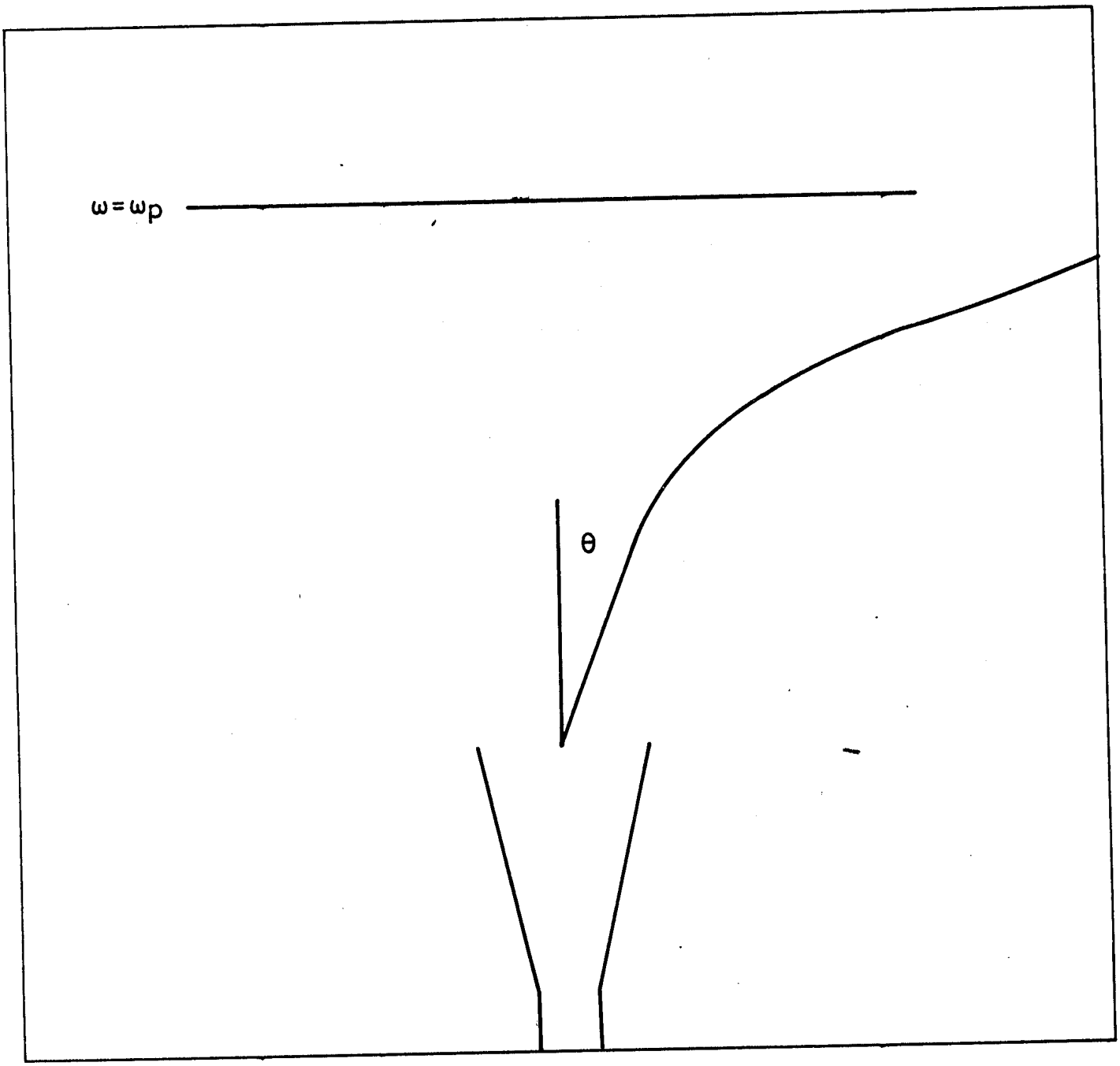


Fig. 9

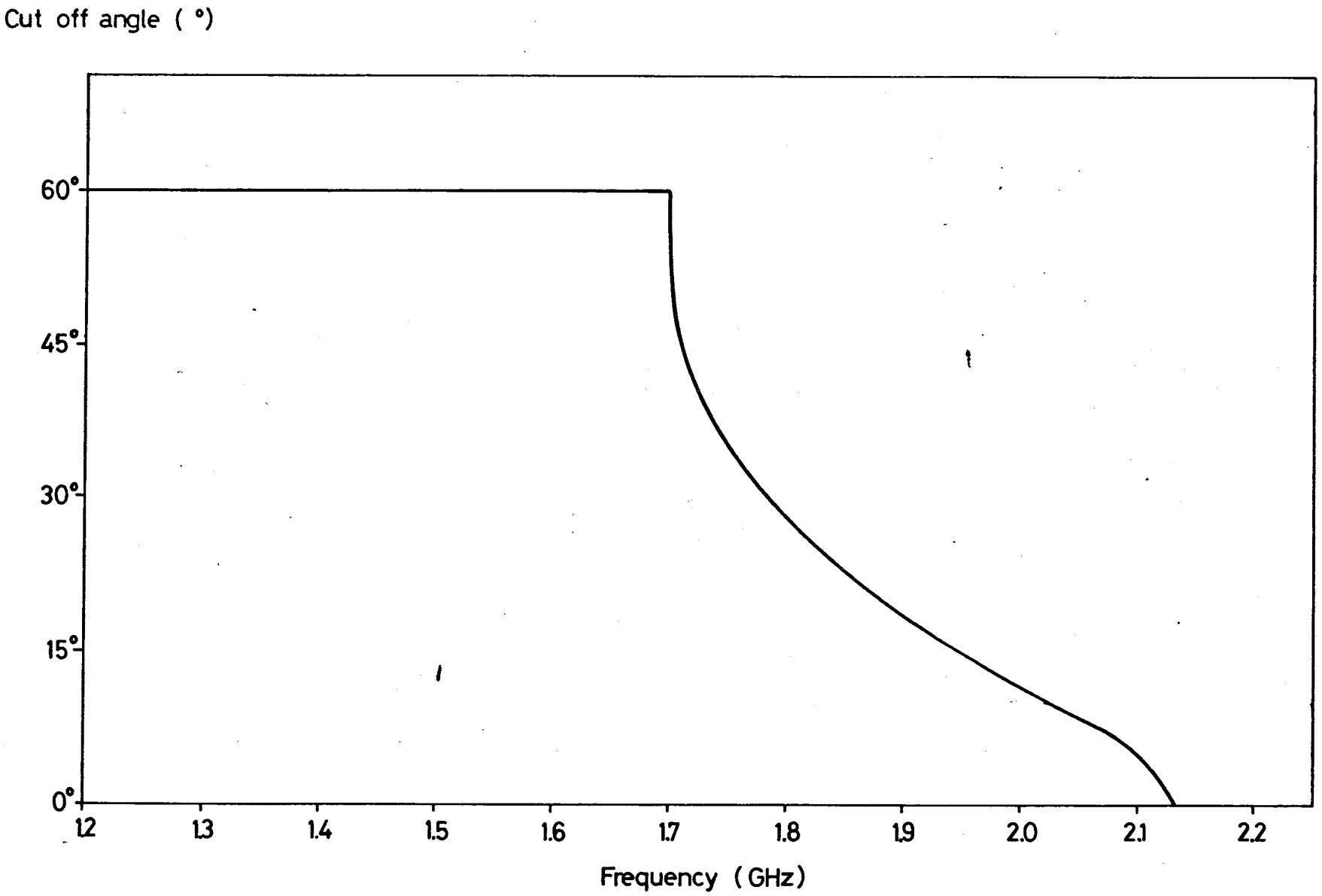
Cut off angle ( °)
60°
45°
30°
15°
0°
1.2
1.3
1.4
1.5
1.6
1.7
1.8
1.9
2.0
2.1
2.2
Frequency (GHz)

Fig. 10

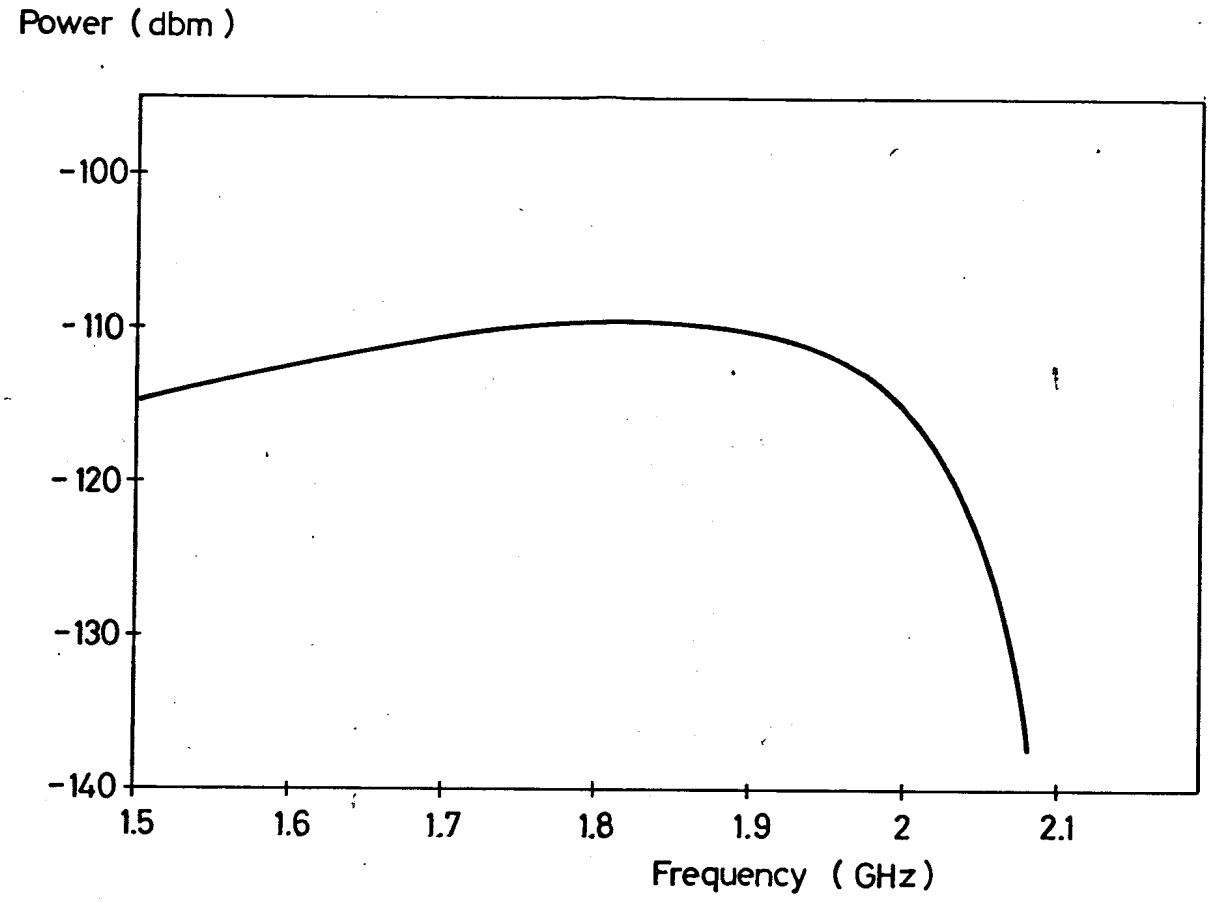


Fig. 11

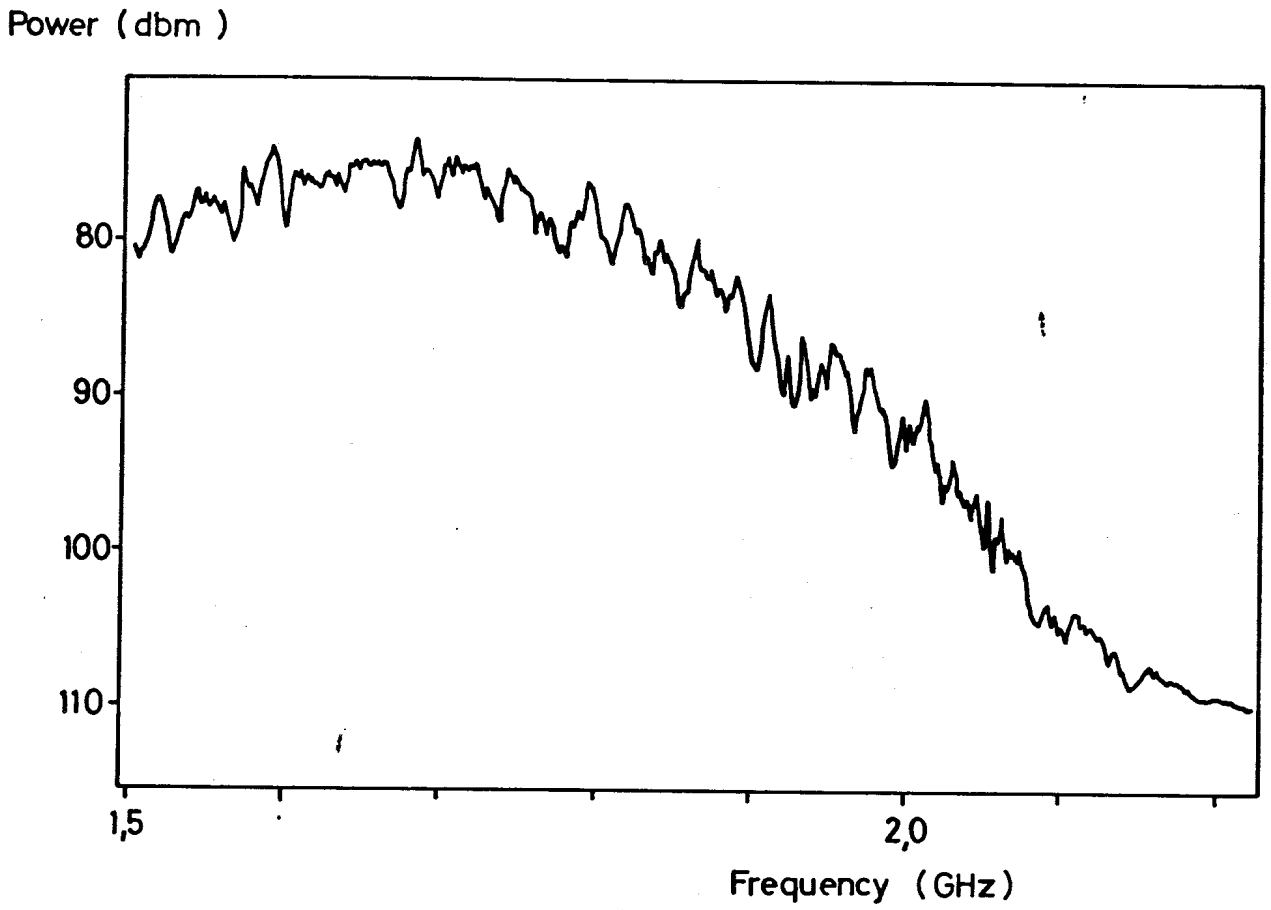


Fig. 12

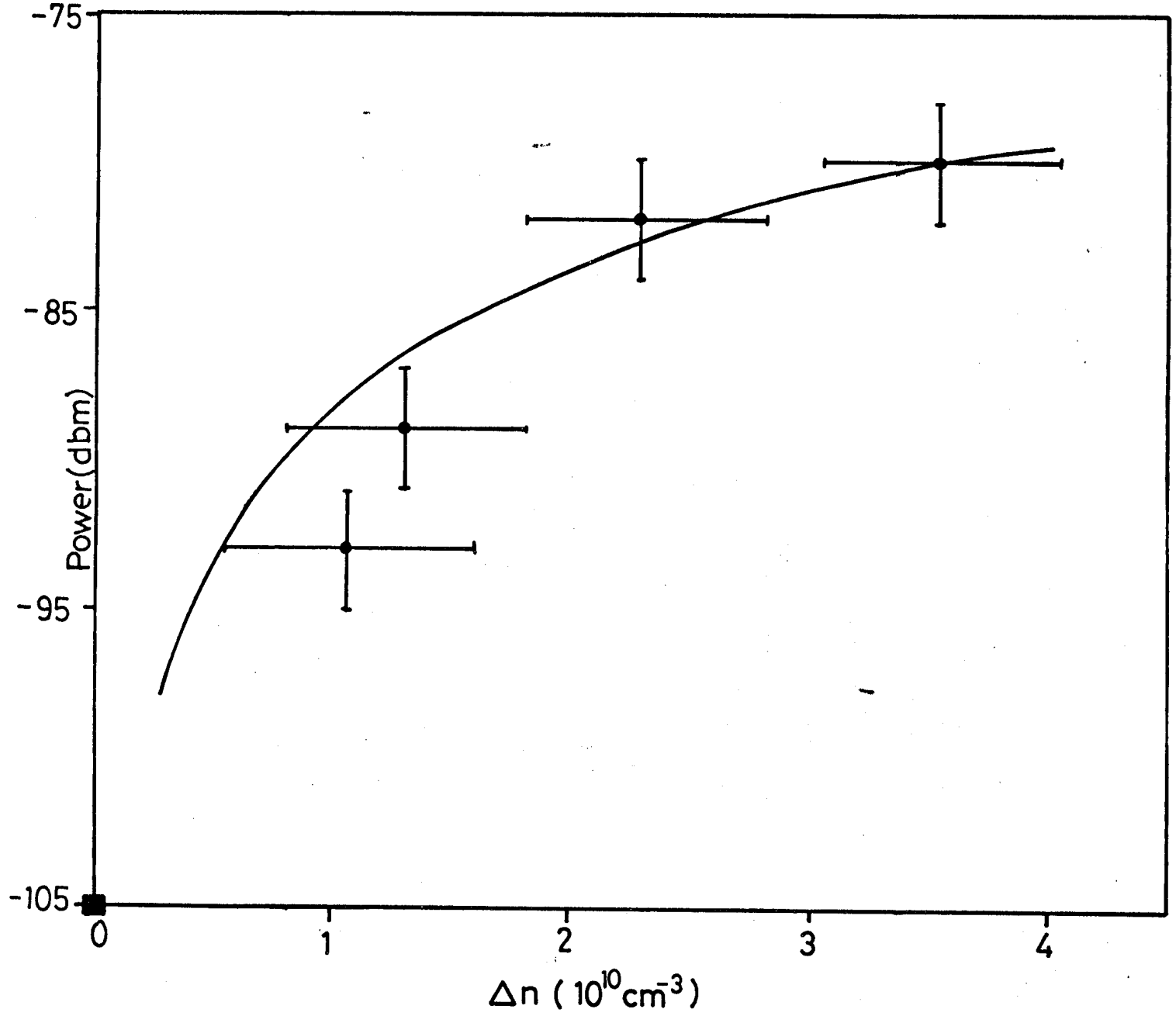


Fig. 13

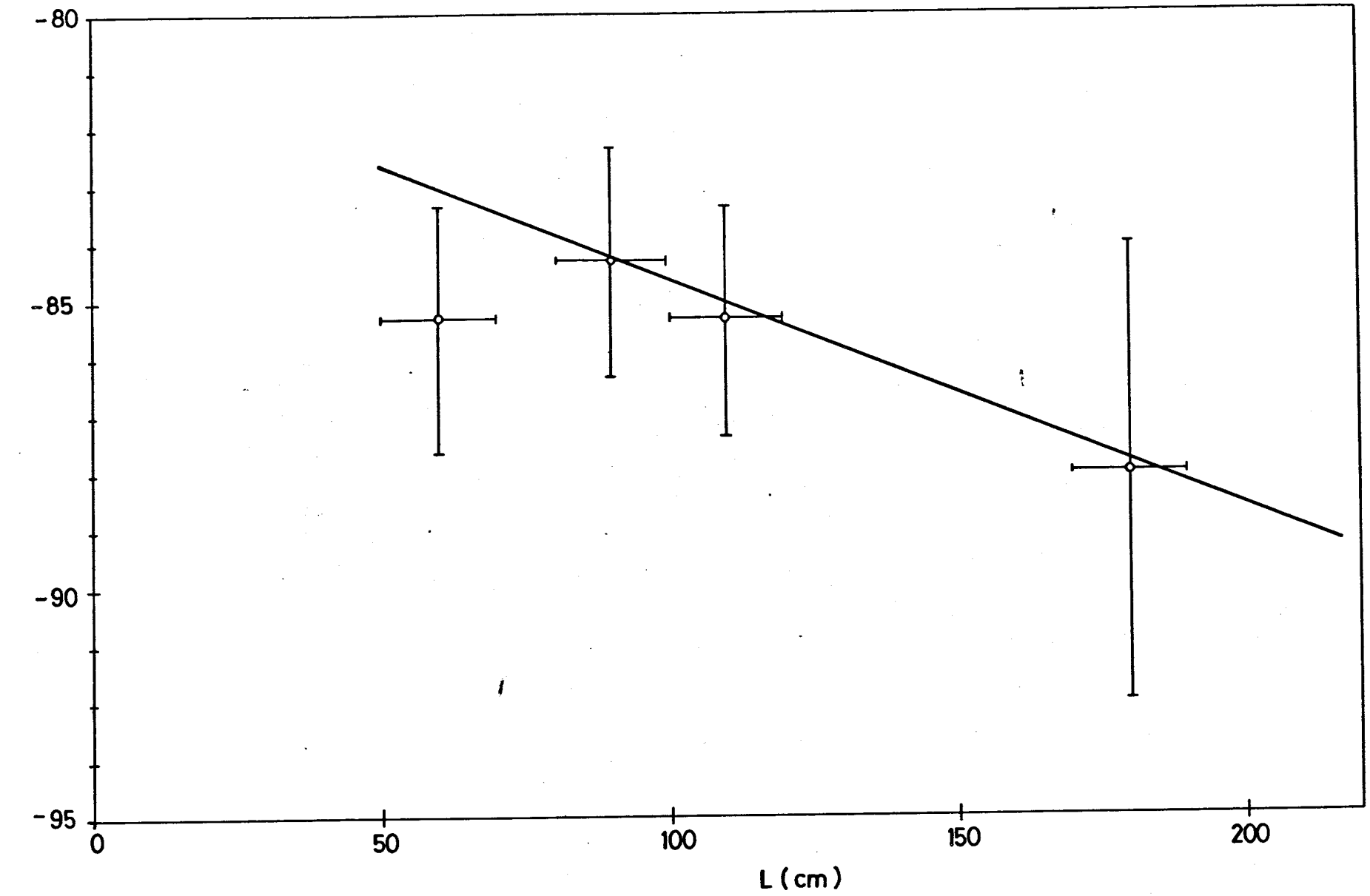


Fig. 14

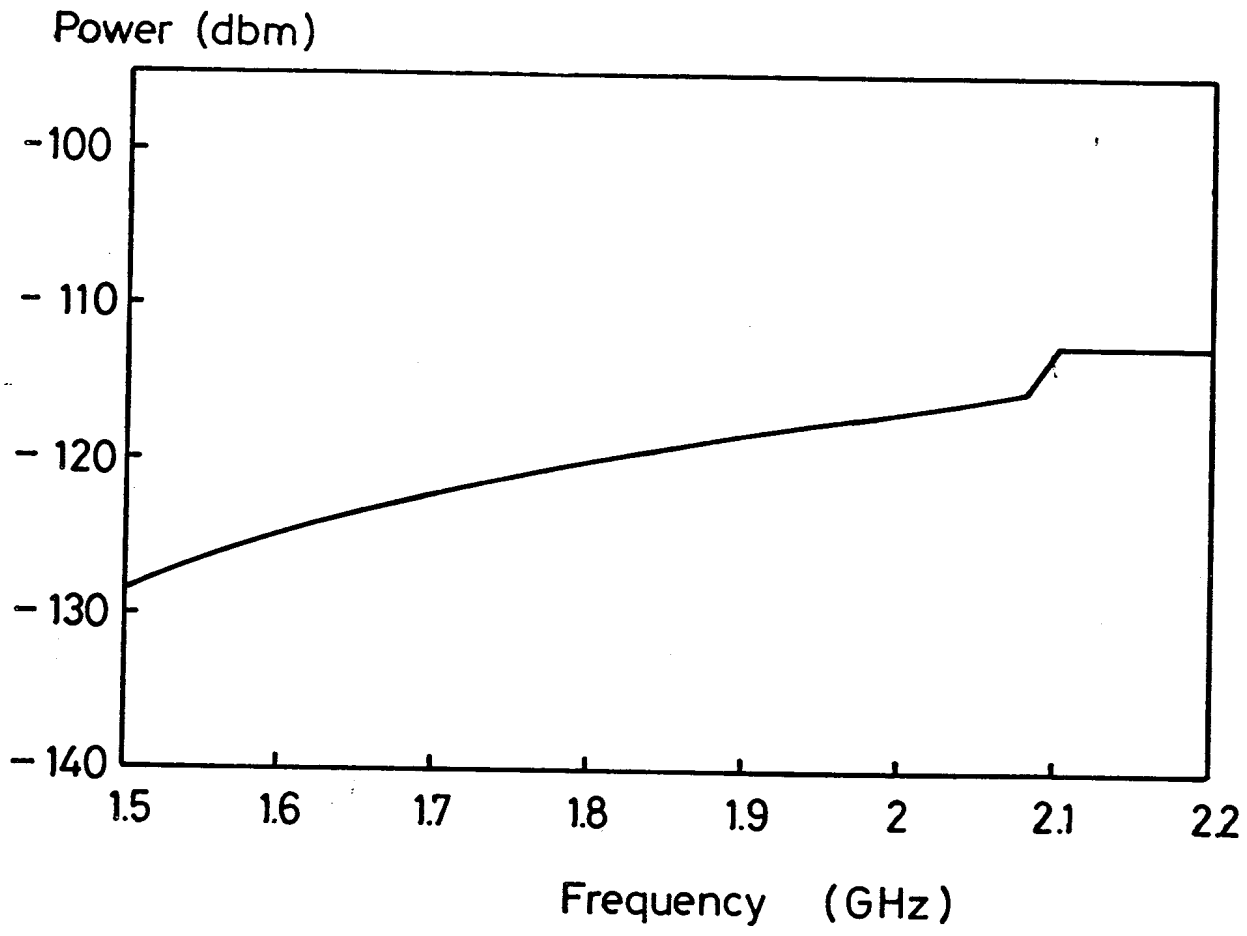
Power (dbm)
-100
- 110
- 120
- 130
- 140
1.5
1.6
1.7
1.8
1.9
2
2.1
2.2
Frequency (GHz)

Fig. 15

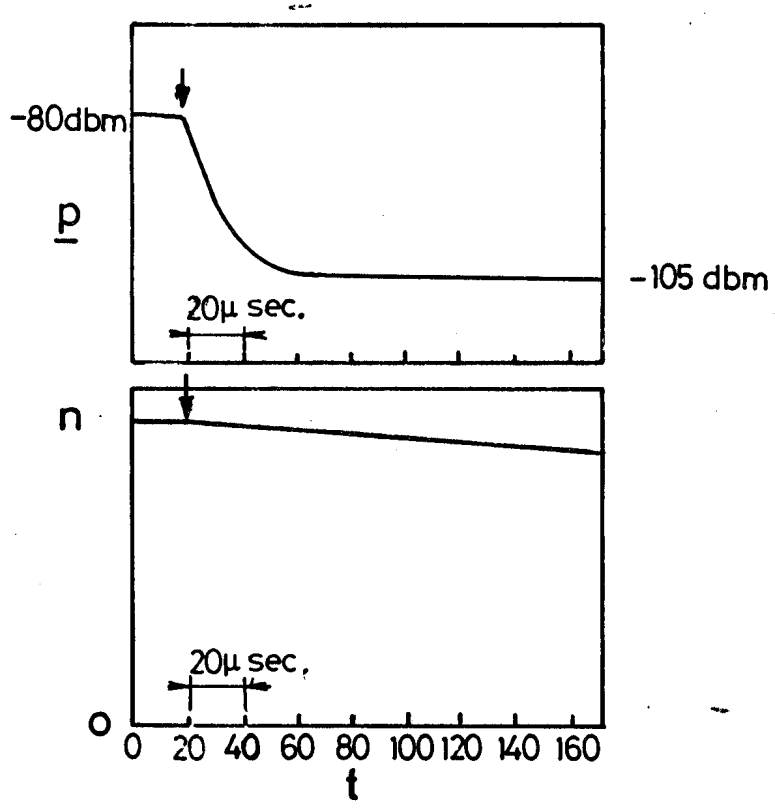


Fig. 16